

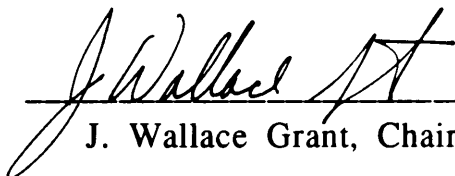
Characterization of Adhesively
Bonded Joints Using
Bulk Adhesive Properties

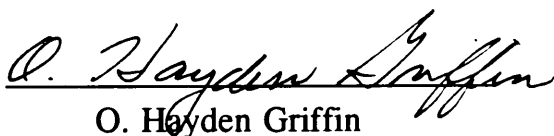
Haruhiko Kon

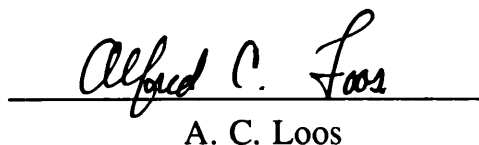
Thesis respectfully submitted to the faculty of the
Virginia Polytechnic Institute and State University
in partial fulfillment of the requirements for the degree of

Master of Science
Engineering Mechanics

Approved by:


J. Wallace Grant, Chairman


O. Hayden Griffin


A. C. Loos

October 1991
Blacksburg, Virginia

Spec

LD
5655
V855
1991
K66
Spec

ABSTRACT

Though using bulk adhesive properties to predict adhesively bonded joint response has yet to be proven infallible, based upon the success of previous works, this effort attempts to shed some light on the stresses present in a typical automotive bonded joint. Adhesive material properties obtained in previous works were used in a finite element analysis of a simulated automotive joint to predict the stresses in that joint.

The automotive joint analyzed was a simplified representation of a joint provided by General Motors. The specifications included the rate or stiffness of the joint and the materials to be used. The basic design of the joint is a rectangular solid section steel frame to which an SMC panel is bonded using Ashland Chemical urethane based adhesives.

Due to computer time constraints and problem complexity, a complete analysis including a time dependent, viscoelastic analysis was not possible. The linear elastic case analyzed gave important insight into the magnitudes of stresses to be expected in a typical joint. It was found that for an applied load to produce a 1 degree deflection in the steel frame, the stresses in the adhesive were below 20% of the ultimate tensile strength of the adhesive. This low stress state is significant because the adhesive behaves as a linear

viscoelastic material in that range, making further analysis less complicated and time consuming.

ACKNOWLEDGEMENTS

The author would like to thank those persons whose help, support, and advice made this effort possible, namely and mainly Dr. J. W. Grant, academic advisor and Committee Chairman, for his encouragement and for putting the scope of the work into much needed perspective. Thanks also to the Center for Adhesive and Sealant Science and the Adhesive and Sealant Council for selecting me as the recipient of their respective fellowships during my three years of study, and a special thanks to Dr. J. P. Wightman, CASS Director, for his additional support and confidence. Thanks to General Motors Corporation and Ashland Chemical Company for funding this project and for technical support. Thanks to SDRC's I-DEAS Hotline for their patient and consistent aid in overcoming the numerous obstacles encountered while using their code.

On a lighter note, the author would like to thank the people and places whose willing and unwitting contributions to my graduate life often made the unbearable times quite bearable. Some of those that come to mind, in no special order are: Dave C., Lorraine, The Cellar, Hannes (Heintz), Honda Motorcycles, North Fork Trading Co., Jon N., Sam, Andy B., Ton 80 Club, Cortney, The Balcony, 117 S. Main Cafe, B.J., Stevie Ray Vaughan, the Simpsons, and most recently, SC@VT and their members Bhaba, Dave F., Kami, Dave S.....

TABLE OF CONTENTS

ABSTRACT	ii
ACKNOWLEDGEMENTS	iv
TABLE OF CONTENTS	v
LIST OF FIGURES	vi
LIST OF TABLES	vii
1.0 INTRODUCTION	1
2.0 BACKGROUND INFORMATION	6
2.1 Theory of Viscoelasticity	6
2.1.1 Linear Viscoelasticity	8
2.1.2 Nonlinear Viscoelasticity	12
2.2 Finite Element Analysis	18
2.3 Previous Work	20
3.0 ANALYSIS & RESULTS	23
3.1 Automotive Bonded Joint Model	26
3.2 Results & Discussion	35
4.0 CONCLUSIONS	46
REFERENCES	48
APPENDIX A	51
APPENDIX B	55
APPENDIX C	58
VITA	85

LIST OF FIGURES

Fig. 1.0: Interphase layer in typical adhesively bonded joint	3
Fig. 2.0: Mechanical analog design elements for modelling linear viscoelastic materials	11
Fig. 3.0: Isochronous stress-strain curve	13
Fig. 4.0: Schematic of automobile joint	29
Fig. 5.0: 10-node solid parabolic tetrahedral element	31
Fig. 6.0: Load and restraint conditions on joint	34
Fig. 7.1: Peel stress range through bond thickness of 55 ksi adhesive due to shear loading (Load Case 1)	40
Fig. 7.2: Peel stress range through bond thickness of 5 ksi sealer due to shear loading (Load Case 1)	40
Fig. 7.3: Peel stress range through bond thickness of 55 ksi adhesive due to torque loading (Load Case 2)	41
Fig. 7.4: Peel stress range through bond thickness of 5 ksi sealer due to torque loading (Load Case 2)	41
Fig. 7.5: Shear stress range through bond thickness of 55 ksi adhesive due to shear loading (Load Case 1)	42
Fig. 7.6: Shear stress range through bond thickness of 5 ksi sealer due to shear loading (Load Case 1)	42
Fig. 7.7: Shear stress range through bond thickness of 55 ksi adhesive due to torque loading (Load Case 2)	43
Fig. 7.8: Shear stress range through bond thickness of 5 ksi sealer due to torque loading (Load Case 2)	43

LIST OF TABLES

Table 1.0: Material Properties of Polyurethane Adhesives Exhibiting 20% UTS Linear Viscoelastic Limit	24
Table 2.0: Material Properties of Model COmponents	28
Table 3.0: Absolute Stress Ranges for the Adhesive Layer for Each Loading Condition	38

1.0 INTRODUCTION

The use of adhesives in industry has greatly increased since their introduction into the aerospace industry in the early 1940's. In fact, according to 1989 estimates, the demand for adhesives was expected to exceed the growth rate of the GNP by 250% in the automotive industry. The reasons for this increase in popularity are many; most notable are the many advantages derived from using adhesives over conventional fastening methods [13].

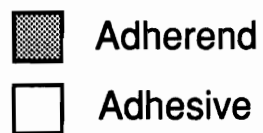
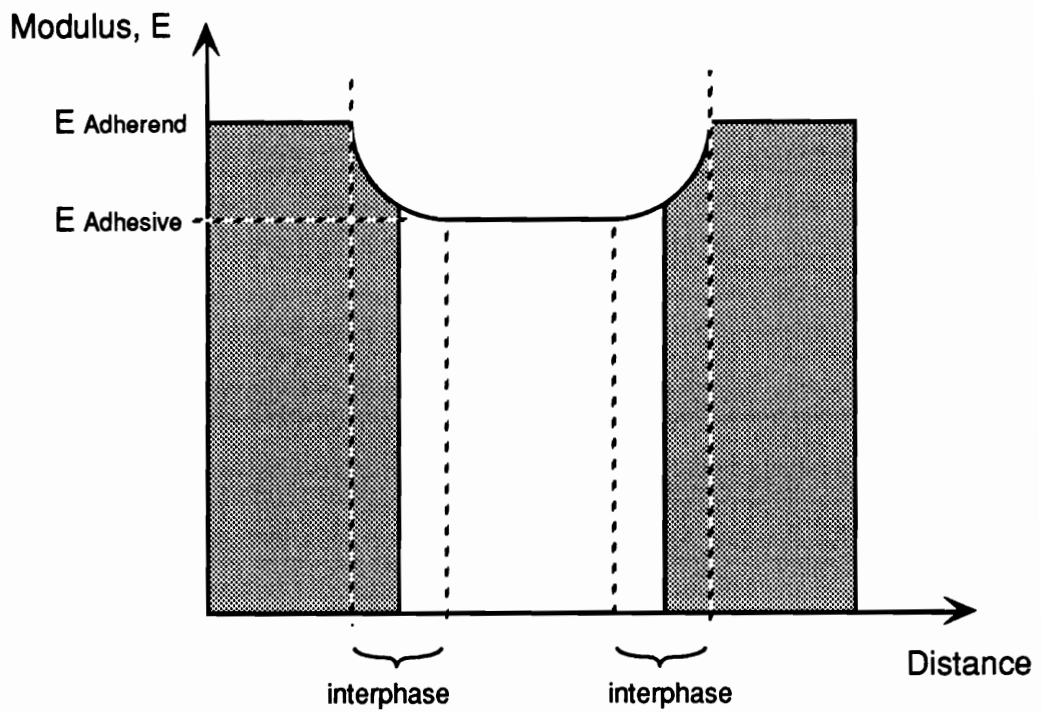
The use of conventional fasteners requires that the constituent parts have holes whether they are drilled, punched, or molded in to the material. These holes are areas of very high stress concentrations which are undesirable in any design. In composite materials the problem is compounded by inevitable fiber damage due to drilling.

By adhesively bonding parts together, most of the stress concentrations are eliminated, thus promoting a far more uniform stress distribution and consequently, a stronger joint. Adhesively bonded joints are not rigid, as conventionally fastened joints are, which implies that they are tougher and not as susceptible to fatigue failures when subjected to cyclic loads, i.e. there are no bolts or rivets to shear or vibrate loose.

Other advantages to using adhesives include their utility in joining dissimilar materials, e.g. metals where conventional fasteners might cause a galvanic reaction. Adhesives, during application, automatically seal the joint, insuring a water/air tight joint without the use of additional sealers. Adhesives eliminate fasteners entirely, which yield great savings in production and inventory costs

There are, however, problems associated with using adhesives. Adhesives are polymers and as a general rule, polymers are affected by environmental factors such as temperature, moisture, and pollutants. Polymers also exhibit viscoelastic behavior, i.e. their deformation behavior is time dependent as well as stress dependent. Therefore it is very important to assess the environmental as well as load conditions under which adhesives are to be used and decide whether or not their use will be effective and advantageous.

The greatest problem with using adhesives in structures is the difficulty in determining the in-situ behavior of the joints. It is very curious to note that in today's automotive industry, where pioneering efforts in adhesively bonding vehicles together are being made, little is known about the actual stresses in those bonded joints. The main reason for this lack of information is because an adhesively bonded joint's mechanical properties are a mix of properties contributed from both constituents of bulk and interfacial curing of the adhesive-adherend system. An adhesively bonded joint is generally made up of high modulus adherends and a lower modulus adhesive. An interesting phenomenon exists at the adhesive-adherend interface.



$$E_{\text{Adherend}} > E_{\text{interphase}} > E_{\text{Adhesive}}$$

Figure 1.0 Interphase layer in typical adhesively bonded joint

This interface, commonly referred to as the interphase layer, has material properties whose magnitudes lies somewhere in between those of the adherend and adhesive. This concept is illustrated in Figure 1. The extent to which the interphase layer influences the joint's behavior is difficult to quantify and to this date, no sure method to do so has been established. It is a far easier task to individually characterize the behavior of the adherends and adhesive. In a joint geometry where the bond thicknesses are relatively large, as in the automotive industry, the adhesive properties are more prominent in the joint than would be in a joint found in the aerospace industry, where the bondline thicknesses are quite small and uniform. For these "thick adhesive" joints, it may be feasible to approximate the bonded joint's behavior using the bulk adhesive's material properties.

It is the objective of this work to apply this approach to a more practical scenario. By incorporating the material properties of an automotive adhesive into a finite element analysis, it may be possible to approximate the behavior of the adhesive in a bonded joint. This effort focussed on two automotive adhesives supplied by Ashland Chemical Co.: PG-1 and a generic sealer, identified only by its material properties, which are both two-part urethane adhesives. Joint specifications supplied by General Motors Corp. were incorporated into a simplified model of a bonded automobile joint and subjected to shear and torsional (warp) loading conditions. This

model was then analyzed using F.E.A. methods to predict the stress distributions in a typical automobile joint.

The two finite element analysis codes used were developed by Hibbitt, Karlsson, and Sorensen, Inc. and Structural Dynamics Research Corporation called, respectively, ABAQUS and I-DEAS.

2.0 BACKGROUND INFORMATION

2.1 THEORY OF VISCOELASTICITY

The behavior of all materials can be characterized through the use of three types of equations. The first set of equations relates the stresses or forces on a body with the loads placed upon it. For linear problems, these relationships are known as equilibrium conditions. For nonlinear or dynamic problems, they are referred to as the equations of motion. The general form of the equations is as follows:

$$\sigma_{ji,j} + \rho f_i = 0 \quad i, j = 1, 2, 3 \quad (1)$$

σ_{ij} is stress, ρ is the density of the body and f is the body force.

The second group of equations relates the strains on a body to their respective displacements. These relations are called the kinematic conditions or strain-displacement equations which in general form can be written,

$$\epsilon_{ij} = \frac{1}{2} \left(\frac{\partial u_i}{\partial y_j} + \frac{\partial u_j}{\partial y_i} \right) \quad i, j = 1, 2, 3 \quad (2)$$

where u is displacement and y is the global coordinate.

The third group of equations gives the relationship between the displacements/strains to the loads/stresses on a body. These relations are material dependent and are the equations which determine the behavior of the material. These equations are known as the constitutive equations. For linear elastic materials, where the strains are a linear function of stresses, the constitutive equations are a set of six equations collectively known as Hooke's Law:

$$\epsilon_{ij} = S_{ijkl} \sigma_{kl} \quad i, j, k, l = 1, 2, 3 \quad (3)$$

S_{ijkl} is the fourth order tensor for compliance.

However, not many materials can be characterized so simply. Most materials are affected by other factors such as loading rate or strain rate and even the stress level. These time and stress dependent materials are classified as viscoelastic, and may be further subdivided into two groups: Linear viscoelastic and nonlinear viscoelastic materials.

2.1.1 Linear Viscoelasticity

The response to a load on materials classified as linearly viscoelastic varies only with time. Two phenomena which exemplify this type of behavior are creep and stress relaxation. Given a constant load, a viscoelastic material will respond with an initial instantaneous strain. Maintaining this load over time causes the material to continue to elongate gradually until the strains reach the material's limitations. This transient response to a constant load is called creep. Similar to creep, stress relaxation is the phenomenon observed when the material is subjected to a constant displacement. Over time, the stresses in the material drop, rapidly at first, then slowing asymptotically to a material dependent level. The constitutive equation for a linearly viscoelastic material under a constant load can be written

$$\epsilon_{ij}(t) = S_{ijkl}(t) \sigma_{kl} u_c(t) \quad i, j, k, l = 1, 2, 3 \quad (4)$$

where $u_c(t)$ is a unit step function at time $t = c$. Naturally this equation can be generalized to include all types of loadings:

$$\epsilon_{ij}(t) = \int_{-\infty}^t S_{ijkl}(t-\tau) \frac{d\sigma_{kl}(\tau)}{d\tau} d\tau \quad (5)$$

Equation 5 is commonly called the Boltzman integral. The similarity between the linear elastic constitutive equation, Eq. 3, and the viscoelastic constitutive equation, Eq. 4, is apparent; the only difference being the time dependence of the viscoelastic creep compliance.

Another way of modelling linear viscoelastic materials is through the use of two basic mechanical analog elements: The spring element and the dashpot element. The spring element is purely elastic, i.e. it reacts instantaneously to a load but has an elastic limit. Its reaction is determined by a spring constant, k , which is associated with the displacement of the spring (Fig. 2.0a). The dashpot element is purely viscous and therefore is sensitive to loading rates and is the element that introduces the viscous, time dependent behavior to a viscoelastic model. There is no instantaneous response and no limit to its elongation potential. Its reaction is governed by a damping coefficient, c , which is associated with the velocity at which the element is loaded (Fig. 2.0b).

By combining a spring and a dashpot either in parallel or in series, the response of the system can be tailored to fit the behavior of a viscoelastic material. Two common "building blocks" for viscoelastic materials are the Maxwell fluid and the Kelvin solid. The Maxwell fluid is a spring and dashpot in series. This type of material has the instantaneous response of a spring and the unlimited displacement of a dashpot (Fig. 2.0c). The Kelvin solid is a spring and dashpot in parallel which gives it the elastic limit of the spring and

the delayed response of the dashpot (Fig. 2.0d). These materials, when generalized and combined in various ways, are capable of modelling the response of a myriad of different viscoelastic materials. Two examples of such materials are the generalized Maxwell fluid and generalized Kelvin solid (Figs. 2.0e & 2.0f). These generalized material elements are able to model more complex behaviors while retaining their fluid/solid response characteristics to a degree that their individual constituent elements cannot. It is plain to see that the possibilities for different combinations of these elements are as numerous as the number of materials available to be modelled.

Analyzing these models is accomplished by assembling the necessary equilibrium, kinematic, and constitutive equations, and then solving the governing differential equation unique to each model. The most important variable in these g.d.e.'s is the time constant of the viscous dashpot because it determines the rate at which the material responds.

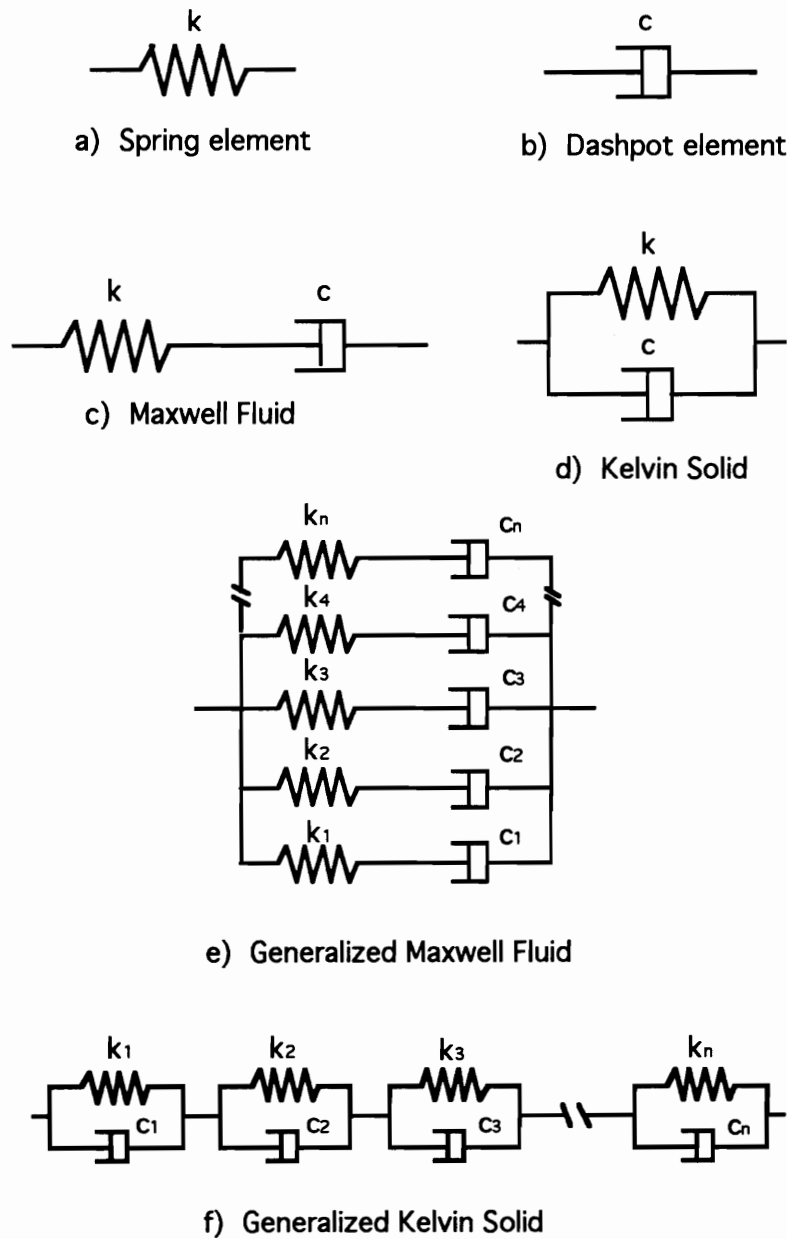


Figure 2.0 Mechanical analog design elements for modelling linear viscoelastic materials

2.1.2 Nonlinear Viscoelasticity

In addition to being time dependent, the response of nonlinearly viscoelastic materials are also stress or load dependent. This means that for a given time, the material will behave differently at varying loads. This concept can be clarified by constructing an isochronous stress-strain curve for both a linear and nonlinear viscoelastic material. This is done by collecting stress-strain data from a series of creep/creep recovery tests at various stress levels and plotting a family of compliance curves at constant times. A family of constant-sloped curves indicates linear viscoelasticity, while a family of nonlinear curves denotes a nonlinear viscoelastic response (Fig. 3.0).

Modelling nonlinear viscoelastic materials is considerably more difficult than doing so with their linear counterparts. Though it is possible to model a nonlinear response using spring and dashpot elements, their time constants become functions of stress and time, making solving the resulting differential equation of motion a very cumbersome and undesirable task.

More suitable for modelling nonlinear viscoelastic materials are the following four methods. The first two methods are based on the Boltzman convolution integral used to model linear viscoelastic

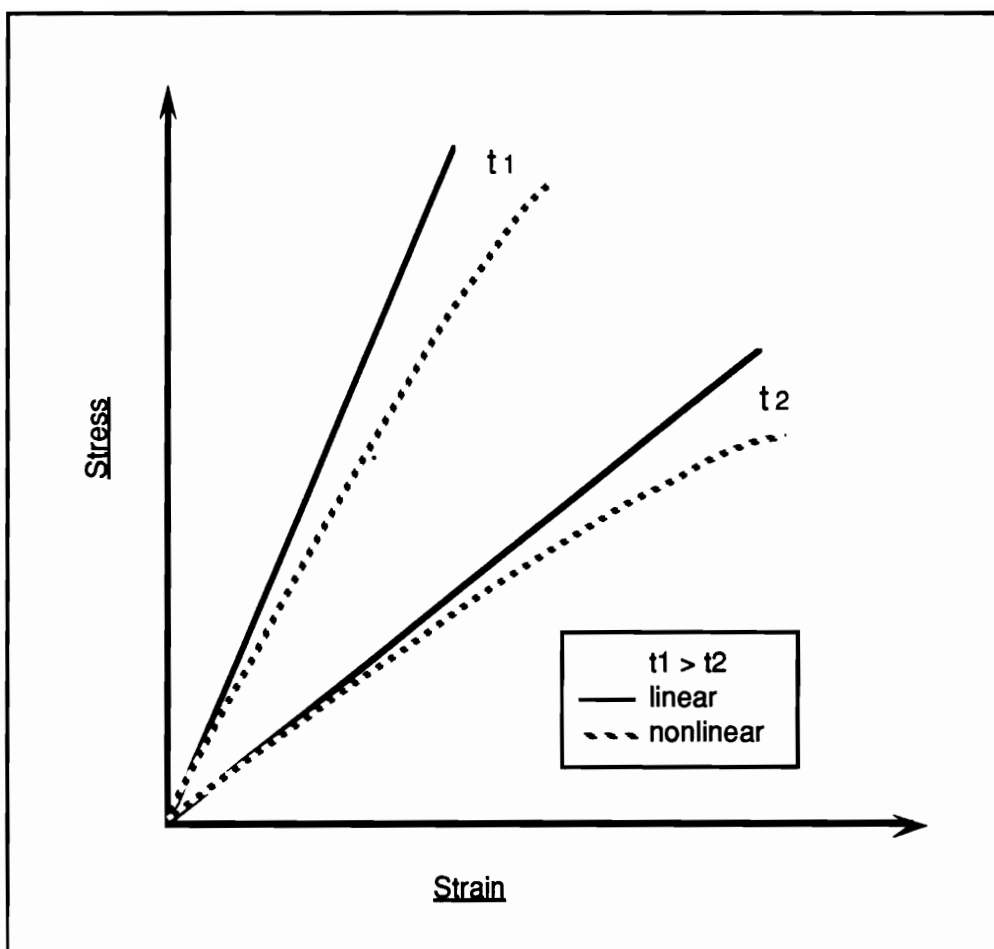


Figure 3.0 Isochronus Stress-Strain Curve

responses. The Green-Rivlin approach [9] uses multiple convoluted integrals and is of the form,

$$\begin{aligned} \epsilon(t) = & \int_{-\infty}^t D_1(t-\tau) \frac{d\sigma(\tau)}{d\tau} d\tau \\ & + \int_{-\infty}^t \int_{-\infty}^t \int_{-\infty}^t D_3(t-\tau_1)(t-\tau_2)(t-\tau_3) \frac{d\sigma(\tau_1)}{d\tau_1} \frac{d\sigma(\tau_2)}{d\tau_2} \frac{d\sigma(\tau_3)}{d\tau_3} d\tau_1 d\tau_2 d\tau_3 \quad (6) \end{aligned}$$

where the second term describes the nonlinear viscoelastic effect. Though this method appears very generalized, it is not widely used due to the number of kernel functions, D_1 and D_3 , which must be experimentally determined. The inordinate amount of time necessary to implement this method makes this approach impractical.

The Schapery integral approach [16] is based on thermodynamic principles. The constitutive equation for uniaxial stress is of the form,

$$\epsilon(t) = g_0 D_0 \sigma + g_1 \int_{-\infty}^t \Delta D(\psi - \psi') \frac{d(g_2 \sigma)}{dt} d\tau \quad (7)$$

where D_0 is the initial compliance and $\Delta D(\psi)$ is the transient compliance. The reduced time parameters, ψ and ψ' , are of the form,

$$\begin{aligned}\psi &= \psi(t) = \int_0^t \frac{dt'}{a_\sigma} \\ \psi' &= \psi'(\tau) = \int_0^\tau \frac{d\tau'}{a_\sigma}\end{aligned}\tag{8}$$

where g_0 , g_1 , g_2 , and a_σ are nonlinear functions of stress. Creep and creep recovery data are used to determine these parameters. This procedure is documented by Tuttle [17]. Apparently, the Schapery approach is only applicable to cases with the same load history, i.e. the parameters g_0 , g_1 , g_2 , and a_σ obtained from a creep/creep recovery test may not be valid for modelling a variable stress/load history.

The final two approaches are called power law methods. Findley [5] modified the power law used in linear viscoelasticity so that it could account for nonlinear behavior. The strain, defined as a function of time and stress, is written,

$$\epsilon(t, \sigma) = \epsilon_0^* \sinh(\sigma/\sigma_e) + m^* \sinh(\sigma/\sigma_m) t^n\tag{9}$$

where n is a constant and ϵ_0^* , m^* , σ_e , and σ_m are material constants which must be experimentally determined. The Findley power law is an empirical method which is easy to use. However, due to the presence of hyperbolic functions, numerical schemes often fail for high values of stress.

The quadratic power law developed by Gramoll [8] eliminates this problem by replacing the hyperbolic functions with quadratic functions:

$$\varepsilon(t, \sigma) = (1 + g\sigma^2) \varepsilon_0 + (1 + f\sigma^2) m t^n \quad (10)$$

where g and f are the nonlinear material constants. Again, these constants are determined experimentally. Note that for the case where g and f are zero, the constitutive equation becomes that for linear viscoelasticity. Because of its relative simplicity and lack of major sources of complications in numerical schemes, the quadratic power law will be used to model the nonlinear viscoelastic adhesive in this study.

In order for a constitutive model to be truly effective, it must be able to account for various loading histories. In its present form, the quadratic power law can only handle constant loads. In order to expand its use to, for example, multi-step loadings, some form of superposition principle must be introduced. As implied earlier, both the Green-Rivlin and Schapery models, though applicable to varying stress states, are by nature too difficult to implement to be practical.

Findley and Khosla [5], and later, Findley and Lai [6] proposed superposition principles based on the Boltzman superposition integral. The initial effort modelled experimental data well, but was found to be unusable for certain load cases. This is documented well by Dillard [3]. The latter effort produced something more promising:

$$\begin{aligned}\varepsilon(t) = & [\varepsilon_0(\sigma_0) + m(\sigma_0)t^n] \\ & + [\varepsilon_0(\sigma_1) + m(\sigma_1)(t-t_1)^n - \varepsilon_0(\sigma_0) + m(\sigma_0)(t-t_1)^n] + [\dots] \quad (11) \\ & + [\varepsilon_0(\sigma_i) + m(\sigma_i)(t-t_i)^n - \varepsilon_0(\sigma_{i-1}) + m(\sigma_{i-1})(t-t_{i-1})^n]\end{aligned}$$

where the constants ε_0 and m are the same as in the Findley power law, Equation (9). σ_0 is the initial stress, and σ_i is the stress applied at time t_i for i steps in stress. The validity of this superposition principle is, as yet, untested for very complex load histories and so, its use should be carefully considered.

2.2 FINITE ELEMENT ANALYSIS

Once a suitable viscoelastic constitutive model for a material has been chosen, the next logical step is to check its validity by comparing the analytical results for a test geometry with specific loading and boundary conditions to actual experimental data. There are several methods used to obtain the analytical solution including the finite-difference method, variational method, and finite element method.

The finite-difference method is generally limited to very simple geometries with straight boundaries and the accuracy of the solution is highly dependent on the accuracy of the initial guesses at the solution at discrete points on the model.

Analytical solutions through variational methods are obtained by solving an equivalent variational form of the governing equation by minimizing the quadratic functional of the equation. Once the quadratic functional, actually the total potential energy in the system, has been minimized, the solution to the variational form converges to the exact solution of the original differential equation. This method is useful only for problems for which the domain is clearly defined.

Finite element methods are implemented by applying a variational method in a piecewise fashion to a geometry divided into

a mesh of finite, discrete elements. Because each element has clearly defined boundary conditions, this method does not suffer from the same restrictions as do variational methods. The implementation of finite element methods is far too complex and time consuming to be explained properly here, but is well documented by Reddy [15]. Finite element methods, due to its applicability to a wide variety of geometries, is widely used to produce the analytical solutions.

2.3 PREVIOUS WORK

There have been many previous efforts toward the characterization of adhesively bonded joints in recent years. One of the more recent works is a study by Osiroff [12] which focussed on applying and verifying the feasibility of predicting bonded joint responses using bulk adhesive properties. Osiroff's work progressed in the following way.

Ashland's Pliogrip 6600/6620 two-part urethane adhesive was hand-mixed and cast into sheets, cured, and cut into coupons. These adhesive coupons were tested in tension for its material properties including the adhesive's elastic modulus, Poisson's ratio, ultimate tensile strength (UTS), and creep compliance. The adhesive was found to behave as a viscoelastic material; linearly for stress levels below 20% of its UTS and nonlinearly for stresses above. These data were curve-fitted to a constitutive law, developed by Gramoll [8] discussed earlier, called the quadratic power law.

This constitutive law was used to model the adhesive coupon's compliance using a finite element analysis code, ABAQUS 4.5. The analysis produced very good agreement with experimentally collected compliance data and, therefore, was expanded to test the adhesive model's validity for a bonded joint. The Arcan specimen was chosen for its unique characteristic of producing an almost pure

shear state, which introduces as few complicating out-of-plane stresses as possible. The Arcan finite element analysis results did not agree as completely as did the bulk adhesive analysis, but were adequate and encouraging nonetheless.

Kohl [10], in an unpublished work, studied the bulk adhesive properties of Ashland's PP-1, a two-part urethane adhesive, and PP-2, a two-part toughened epoxy, using DuPont's Dynamic Mechanical Analyzer (DMA). It is noted in industry literature that the DMA is only applicable for testing in the linear range of a material's response. However, PP-1, like Pliogrip 6600/6620, was found to be linearly elastic for stress levels below 20% of UTS. Therefore, for lower stress levels, the results from the DMA are thought to be accurate and reliable. PP-1 was found to be a tough material, having an modulus of elasticity of 78.5 ksi and a UTS of 3400 psi. Creep compliance data was also collected at various temperatures, from long term creep behavior and was analyzed using time-temperature superposition principles. It was the expectation that these results would eventually be used in the characterization of adhesively bonded joints.

Cooper [2] studied the single lap shear, thick adherend lap shear, Arcan, and Cone-and-Plate bonded joints using finite element analysis. Each joint geometry was analyzed using a finite element analysis code, VISTA or ABAQUS, and though not compared to experimentally obtained results, revealed many advantages and disadvantages in their designs.

The single lap shear joint is one of the most widely used bonded joint test geometries due to its simplicity, ease of fabrication, and low cost. However, it is thought to be a poor joint for the purpose of trying to characterize joint behavior due to the bending introduced by the eccentric loading and the resulting complex stress states in the adhesive. Finite element analysis of this joint confirmed the presence of a complex stress state, but it continues to be used in industry as a test for an adhesive bond's shear strength both in quality control and in adhesive property evaluation.

The thick adherend lap shear joint is an improvement over the single lap shear joint in that the thicker adherends resist deformation due to the bending moments produced during tensile loading. Shear in the bond approaches a constant value away from the ends of the bond length. This joint geometry appears to be more suitable model for joint behavior characterization.

The Arcan specimen, as noted earlier, is capable of producing an almost pure stress state for the entire bond length. Though the joint is supposed to be rigid, some bending in the adherends was noticed. Errors introduced by this bending were corrected by using a solid dummy specimen and subtracting its response from the bonded joint results. The Arcan specimen has the most appropriate geometry for characterizing shear response in a bonded joint.

It is due to the success of these previous works that an attempt at this work was initiated.

3.0 ANALYSIS & RESULTS

Osiroff's work established that finite element analysis techniques are fairly reliable and accurate for modelling adhesively bonded joints using the adhesive's bulk properties. The research also revealed that for those adhesives tested, below a certain stress level, the adhesive does not respond as a nonlinear viscoelastic material. Kohl studied other similar adhesives and found that this "limit of linear viscoelasticity" existed for his sample as well. Several adhesives' material properties are shown in Table 1.0.

The primary goal of this work was to establish a technique for finding realistic stresses in an automobile sheet molding compound (SMC) to steel frame bonded joint using techniques and results obtained in previous efforts. Using another urethane adhesive similar to those tested previously, this effort is aimed at approximating the stresses in a typical joint present in an automobile through finite element methods.

The joint analysis was performed assuming the adhesive to be a linear elastic material in order to assess the realistic initial stresses in the adhesive layer. If the adhesive stresses are found to be below 20% of its UTS, it is reasonable to assume based upon previous results that the adhesive will behave as a linear, not a nonlinear,

Table 1.0
Material Properties of Polyurethane Adhesives
Exhibiting 20% UTS Linear Viscoelastic Limit

Adhesive	Modulus of Elasticity (E) (ksi)	Ult. Tensile Strength (UTS) (psi)
6600/6620	14.8	1000
9000/9020	55.0	3400
PP - 1	78.5	3400

viscoelastic material; i.e. the material's response is a function of time only, not a function of time and stress. If the adhesive can be modelled as a linear viscoelastic material, great savings in computation time for a transient response analysis can be made.

3.1 AUTOMOTIVE BONDED JOINT MODEL

The automobile joint modelled in this work is a simplified representation of an actual roof pillar joint in use in the General Motors' recently introduced medium production All-Purpose Van (APV). The APV is noteworthy because of its unique and advanced design which includes a lightweight space-frame to which flexible, load-bearing thermoset reinforced reaction injection molding (RRIM) body panels, actually glass-reinforced polyester, are adhesively bonded.

Originally, the analysis was to be focussed on the lift-gate assembly of the APV loaded with its own weight and by its hydraulic lifters. The lift-gate analysis was not continued due to its extremely complicated geometry and because the finite element code in which the mesh was initially created by GM was not compatible to the F. E. codes handily available. Another area of interest included the stresses induced in the frame and bonded body panels by jacking the vehicle up (e.g. for a tire change) and dynamic stresses induced by rough terrain. However, these efforts were also abandoned due to the extremely complex nature of the analysis. In order to realistically predict the adhesive stresses in a bonded joint, it became clear that this initial effort would have to consider a very simple joint geometry.

The specifications of the much simpler roof pillar joint were provided by GM and given in the form of joint stiffnesses or "rates." A rate is defined as the bending moment applied to a joint to cause a flexation or rotation of 1 degree. Based on this information and the knowledge of the materials used in the manufacture of the APV, a "typical" automotive bonded joint's geometry was formulated.

The joint consists of a rectangular solid cross-section (1.0 in. × 0.5 in.) steel frame to which a 0.10 in. thick sheet of SMC is adhesively bonded. The two adhesives considered in this analysis were the PG-1 urethane adhesive (very similar to the 6600/6620 adhesive) and an unnamed sealer, both materials modelled with bond thicknesses of 3.5 mm. The modulus of elasticity and UTS is 55 ksi and 2500 psi for the adhesive and 5 ksi and 900 psi for the sealer. These material properties along with the material properties of the steel frame and SMC panel are shown in Table 2.0. An exploded view of this joint (not to scale) is shown in Figure 4.0.

The joint geometry was calculated using standard strength of materials principles. Knowing the "rate" of the joint and the material properties for steel, calculating the joint geometry and cross section is simple, starting with the cantilever beam bending formula,

$$y = \frac{ML^2}{2EI} \quad (12)$$

where y is the amount of deflection, M is the moment or "rate," L is the length of the beam, E is the modulus of elasticity, and I is the

Table 2.0
Material Properties of Model Components

Material	Modulus of Elasticity (E) (ksi)	Ult. Tensile Strength (UTS) (psi)
Steel	29000	70000
SMC	1920	N/A
PG-1	55.0	2500
Sealer	5.00	900

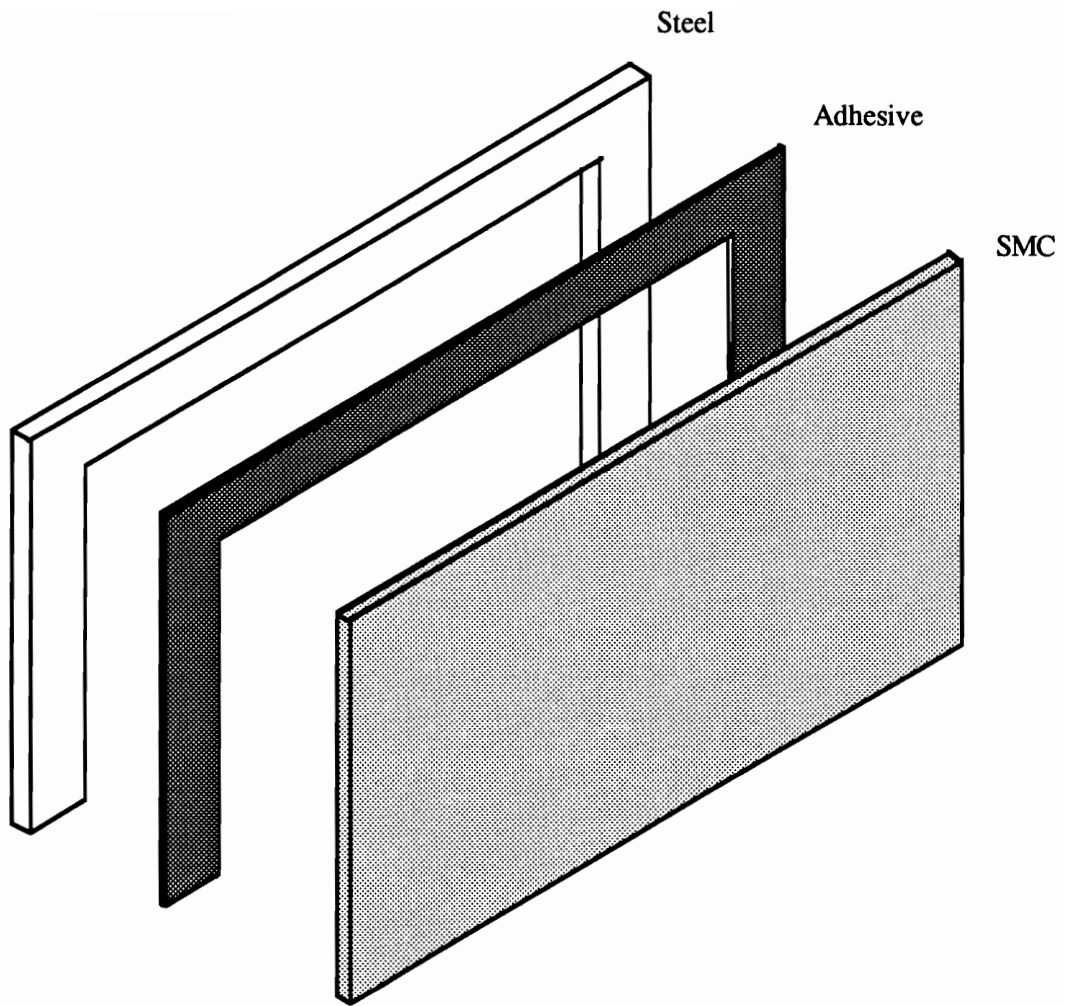


Figure 4.0 Schematic of automobile joint

moment of inertia of the beam cross section. Making the assumption for small deflections, i.e. the value for sine of a small angle is approximately equal to the angle, and solving for the moment of inertia, a suitable beam cross section was determined, as mentioned earlier, to be 1.0" x 0.5".

The F.E. model was generated using S.D.R.C.'s I-DEAS (version V) finite element analysis program. I-DEAS was chosen for pre- and post-analysis because of its menu-driven format and for its very general applicability. Using I-DEAS' Geometry Creation Task, a simple wire-frame of the joint was created according to the dimensions calculated. Using the Mesh Creation Task, a suitable element type was fitted to the wire frame. Two candidate elements were the 8-node solid linear brick element and the 10-node solid parabolic tetrahedral element. The brick element was eliminated because it is not able to accurately model complex geometries deflections in three dimensions. The limited curve fitting capability of linear functions is as well known as the improved fittings obtained when using higher order functions. Similarly, linear elements cannot model complex geometries as well as the higher order parabolic element. The tetrahedral element was chosen to model each of the joint layers for its three dimensional modelling capability and for its relative simplicity. A representation of the element is shown in Figure 5.0 with its node numbering sequence. Each layer consists of two elements through its thickness. This is because it generally takes two tetrahedral elements to make up a quadrilateral shape

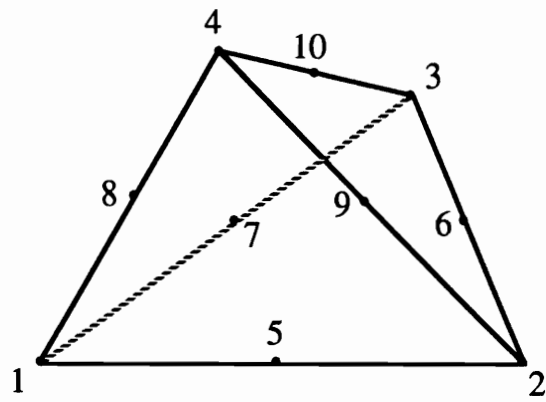


Figure 5.0 10-node solid parabolic tetrahedral element.

required for this model. A view of the elements through the thickness of the model is shown in Appendix A. This brings up the question as to why a 10-node quadrilateral brick element was not used in this analysis. The reason for the element selection made has to do with element aspect ratios. For the relatively thin layers (adhesive and SMC), using a brick element would force the thickness dimension of the element to become quite small relative to the height and width, possibly preventing the analysis converging on a solution. The nodes and elements were generated layer by layer, taking care to keep the nodes at the interface between adjacent layers coincident. Those coincident nodes were then merged, thus creating a model of an ideal adhesive bond. Illustrations of the resulting mesh can be found in Appendix A. This joint geometry is intended to represent one half of a joint, and therefore, the bottom edge of the model is restrained only for translations and allowed to rotate freely. This restraint was applied to the steel frame, adhesive/sealer, and SMC along the lower edge.

This restraint condition may contribute some incorrect stress concentrations in the model at the pinned corners. Because this half-joint model is pinned along its base, it is prevented from deflecting in the y- and z-directions which are expected to produce additional stresses not present in a whole model and accordingly, those stresses should be disregarded. Once the model was completed, it was subjected to two different loading conditions. The first case put the model in shear, and the other was a loading in torsion to warp the

structure (See Figure 6.0). These two loading conditions are intended to create the worst stress states in the model.

The load itself was calculated as the applied force which would cause the frame to rotate 1 degree; a value which corresponds to the “rates” the frame would be subjected during use. From the “rate,” a bending moment, the applied load was calculated simply by dividing by the length of the beam. For the shear loading (Load Case 1), the applied load was calculated as 3055 N (687 lbs). The warp loading (Load Case 2) was approximately 760 N (171 lbs). These loads were distributed across an area of the steel frame as illustrated in Figure 6.0 and were applied in an instantaneous step load for static analysis purposes.

A third loading condition, actually a proposed improvement over Load Case 2, was also considered but not analyzed due to software/hardware compatibility problems. Instead of an applied load to cause the deflection, the warping effect was imposed through nodal displacements which caused a 1 degree rotation of the frame. This new loading condition was intended to eliminate the effects of the applied loads on the frame and anticipated resulting compressive loads in the adhesive and SMC layers.

Once the joint model was completed, it was translated into an ABAQUS input file and analyzed in a single step using ABAQUS version 4.8. The linear elastic analysis results were then read back into I-DEAS using its Dataloader module and studied through I-DEAS' Post Processing Task.

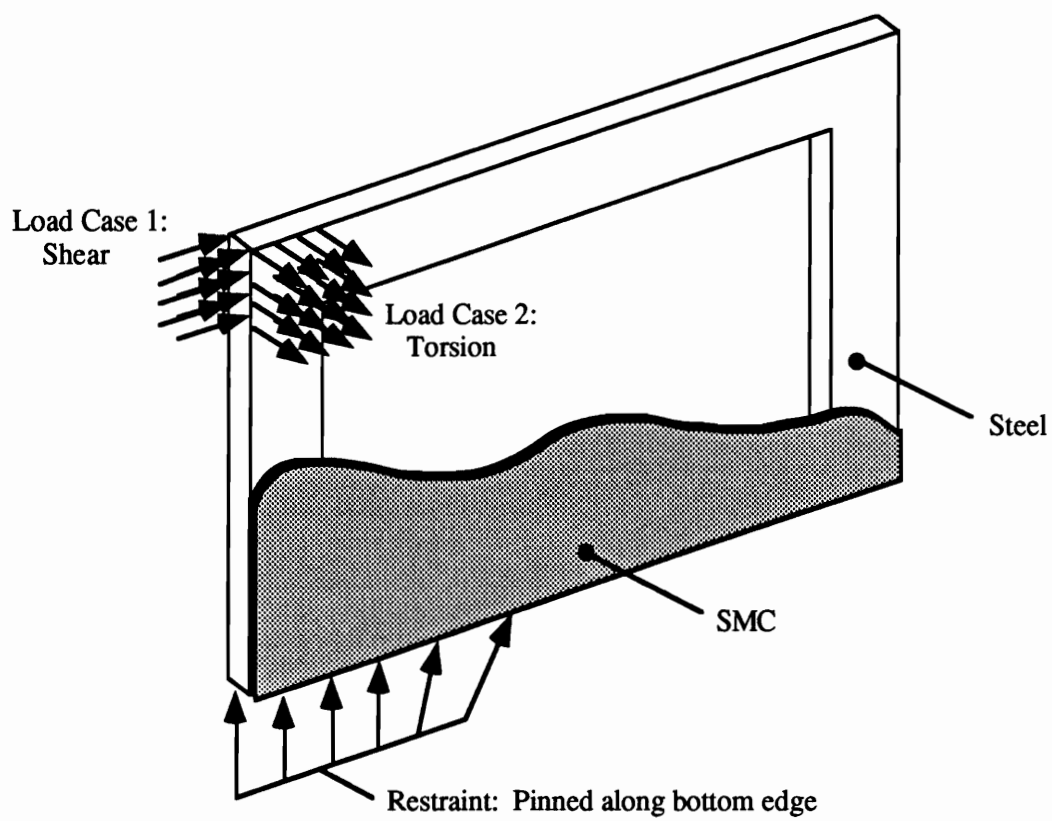


Figure 6.0 Load and Restraint conditions on joint

3.2 RESULTS & DISCUSSION

Most of the results for the automotive bonded joint model were collected in the form of stress contour plots at each layer interface, e.g. at the steel frame/adhesive interface, and at the mid-plane of each layer. Stresses were calculated by ABAQUS for the elements at each integration point or Gauss point for accuracy as opposed to finding the stresses at each node which sacrifices some degree of accuracy. Because this finite element model consists of several layers with different material properties, there is a discontinuity in stresses at the material interfaces. Stresses at these interfaces were analyzed by studying each material layer separately. For example, for this case, the elements that comprised the adhesive layer were grouped together and studied apart from the steel and SMC layers. It would be expected that interfacial stresses for the steel and SMC layers be considerably higher than that for the adhesive layer. Since this effort is concerned mainly with adhesive stresses, only the adhesive layer was studied in detail and discussed here.

Stresses plotted include maximum principle, x-normal, y-normal, z-normal (peel stress), and xy-shear stresses. Maximum principle stress plots for a 3-D analysis did not yield any useful information due to the many stress components included in its calculation, i.e. the plots are too complicated to be of any use in

determining which stress components might cause failure. X- and y-normal stresses are usually not thought of as critical in most joint geometries. The peel stress and shear stress are always important in adhesive bond analysis because peel and shear are the typical adhesive bond failure modes and will be carefully considered in this work.

The analysis results are compiled in the following ways for each loading condition (Load Case 1 & 2) and stress component (peel & shear stresses):

1. Table showing maxima and minima for adhesive & sealer layer. (Table 3.0)
2. Bar graphs of the prominent stress ranges for the adhesive & sealer layer. (Figures 7.1-7.8)
3. Stress contour plots at each interface and at mid-layer planes. (Appendix C)

From this group of data and illustrations, a comprehensive feel for the magnitudes of the stresses, their concentrations, and their trends through the layers of the model can be obtained.

The maximum and minimum stresses for the two adhesives appears fairly consistent from Load Case 1 to Load Case 2. However, the peel stresses for both loading conditions are consistently an order of magnitude greater than the shear stresses (See Table 3.0). The most important piece of information obtained from this data is the fact that the peel stresses are never greater than 4% and 2% of the sealer's and the adhesive PG-1's UTS, respectively. Being below 20%

of the UTS, the materials probably behave linearly, not exhibiting stress dependent behavior.

Figures 7.1-7.8 illustrate how the stress range varies through the adhesive thickness. Note that the stress range considered in these graphs is not the entire range of stresses for the cutting plane, but the range of stresses which covers most of the adhesive area. The thickness of the adhesive/sealer is 3.5 mm with 0.00 at the steel frame interface and 3.50 at the SMC interface. The peel stresses for both Load Cases decreases through the bond thickness, as expected. This trend is due to the steel frame's high stresses and strains which are relaxed in the adhesive layer. It is very interesting to see that the low-modulus sealer and the high-modulus adhesive both behave very similarly under Load Case 1 (shear); stresses being within 20% of each other (Figures 7.1 & 7.2). For Load Case 2 (warp), the similarities also exist, but to a lesser degree (Figures 7.3 & 7.4).

The shear stresses for the high-modulus adhesive are about an order of magnitude greater than for the low-modulus sealer throughout the bond thickness. This is true for both Load Cases 1 and 2. Note that the stress trends for the two cases are opposite one another, i.e. the shear stresses for Load Case 1 are negative at the steel frame interface and become positive towards the SMC interface (Figures 7.5 & 7.6), whereas for Load Case 2, the trend is positive to negative (Figures 7.7 & 7.8). This difference is due to the direction of the loads placed on the model. Load Case 1, the shear load, illustrated in Figure 6.0, causes the model to flex and rotate

Table 3.0

Absolute Stress Ranges* for the Adhesive
Layer for Each Loading Condition

	Peel Stresses [Pa.(psi)]		Shear Stresses [Pa.(psi)]	
Load Case 1	PG-1 Adhes.	Sealer	PG-1 Adhes.	Sealer
Max.	3.39E5 (49.2)	2.51E5 (36.4)	36.0E3 (5.22)	6.0E3 (0.87)
Min.	-4.05E5 (-58.7)	-2.11E5 (-30.6)	-12.5E3 (-1.81)	-7.5E3 (-1.09)
Range	7.44E5 (107)	4.62E5 (67.0)	48.5E3 (7.03)	13.5E3 (1.96)

Load Case 2	PG-1 Adhes.	Sealer	PG-1 Adhes.	Sealer
Max.	3.45E5 (50.0)	1.62E5 (23.5)	36.0E3 (5.22)	7.4E3 (1.08)
Min.	-7.53E5 (-109)	-2.92E5 (-42.3)	-38.0E3 (-5.51)	-8.8E3 (-1.28)
Range	10.98E5 (159)	4.54E5 (65.8)	74.0E3 (10.7)	16.2E3 (2.35)

* Stresses tabulated include those stresses resulting from the model's restraint conditions and may not be accurate for an actual joint. However, any conclusions derived from this data may be considered conservative in its estimation.

in a clockwise direction (when viewed from above). Load Case 2, the torsional load, causes the model to rotate in the opposite direction, thus producing a "mirror image" stress state.

A more qualitative feel for the stresses present in the adhesive layer can be obtained by examining the color stress contour plots which can be found in Appendix C.

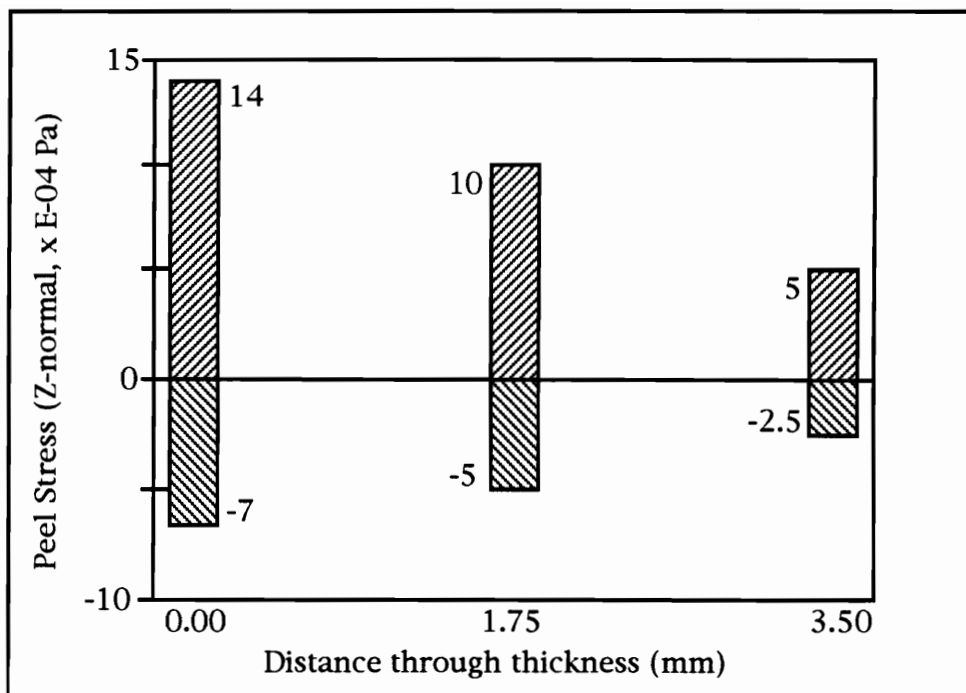


Fig. 7.1 Peel stress range through bond thickness of 55 ksi adhesive due to shear loading (Load Case 1)

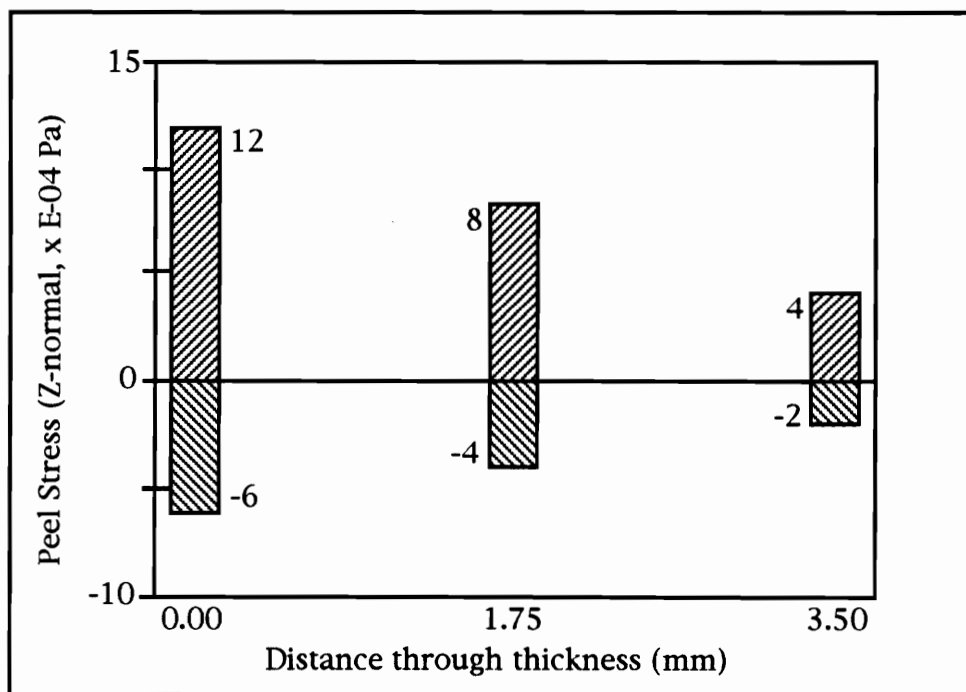


Fig. 7.2 Peel stress range through bond thickness of 5 ksi sealer due to shear loading (Load Case 1)

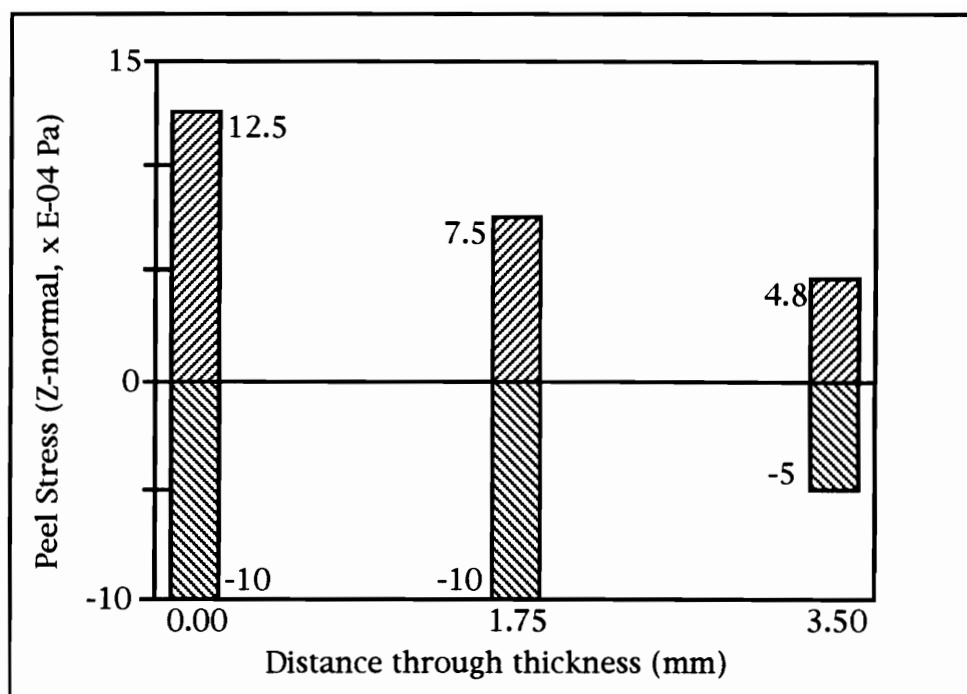


Fig. 7.3 Peel stress range through bond thickness of 55 ksi adhesive due to torque loading (Load Case 2)

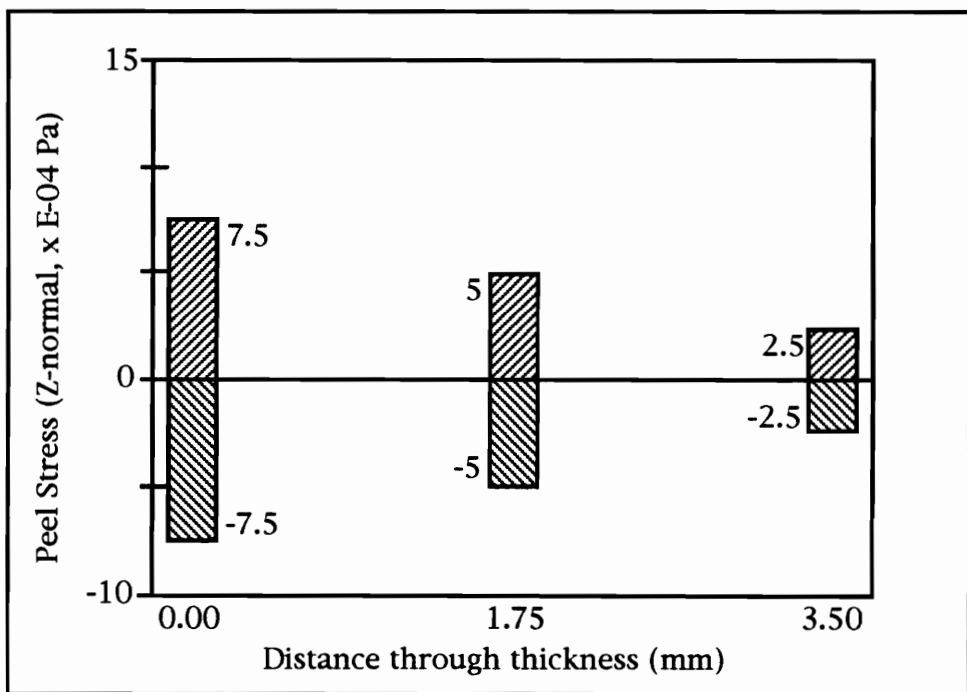


Fig. 7.4 Peel stress range through bond thickness of 5 ksi sealer due to torque loading (Load Case 2)

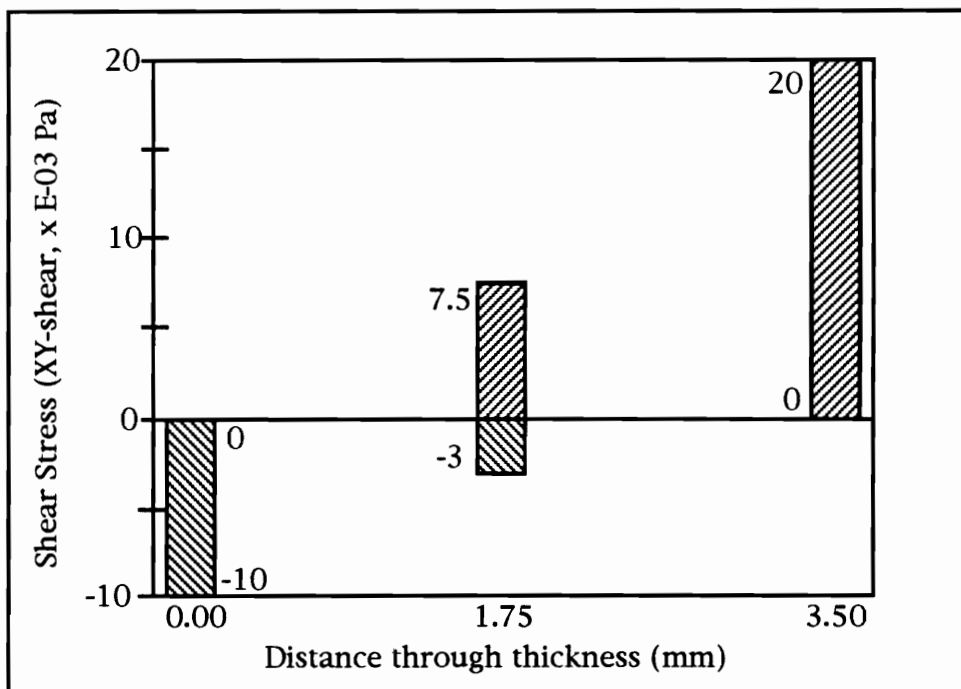


Fig. 7.5 Shear stress range through bond thickness of 55 ksi adhesive due to shear loading (Load Case 1)

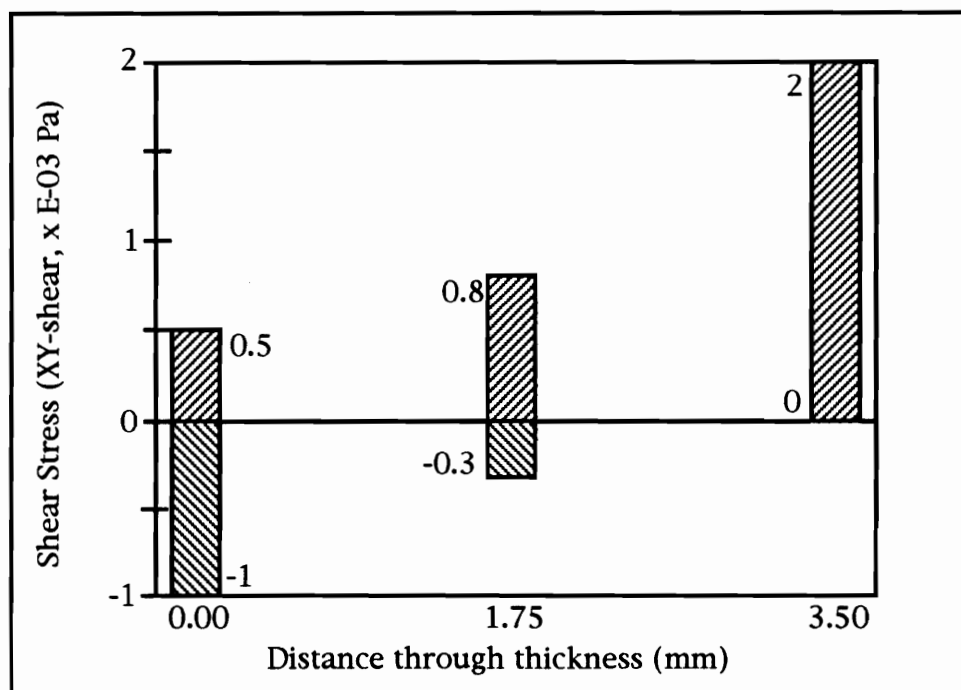


Fig. 7.6 Shear stress range through bond thickness of 5 ksi sealer due to shear loading (Load Case 1)

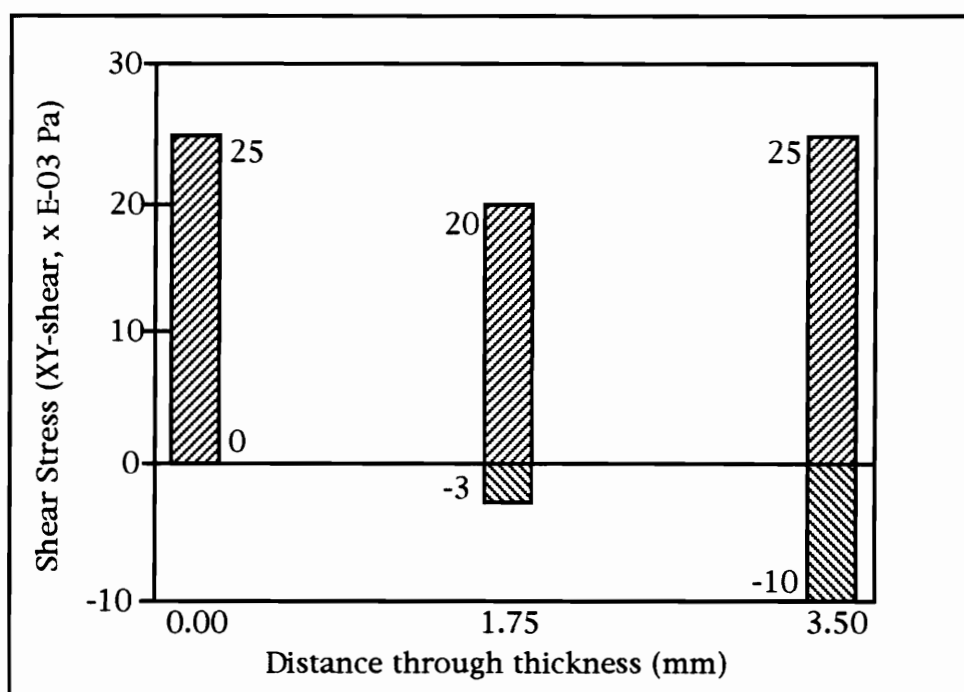


Fig. 7.7 Shear stress range through bond thickness of 55 ksi adhesive due to torque loading (Load Case 2)

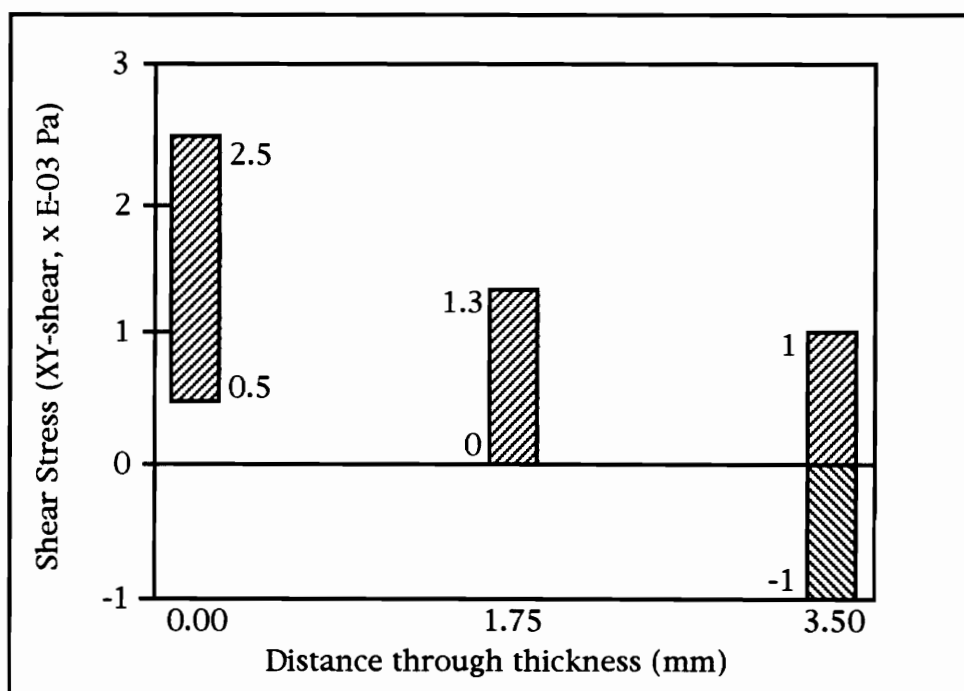


Fig. 7.8 Shear stress range through bond thickness of 5 ksi sealer due to torque loading (Load Case 2)

Note: The analysis was done in SI units and therefore, all stresses in the plots are in Pascals unless otherwise noted.

For Load Case 1, shear stress distributions exhibit a high degree of symmetry. High, or positive, shear stresses are mostly at the SMC interface, especially on the inner half of the adhesive/sealer area. Low, or negative, stresses dominate the steel frame interface.

Peel stress distributions exhibit anticipated stress contours and inflections caused by the twisting of the model. Regions of high (tensile) and low (compressive) stresses occur at the points where the steel frame is forced to twist due to the stiffening effects of the SMC panel. As stated earlier, the highest stresses are present at the frame interface and decrease steadily towards the SMC interface. These high interfacial stresses may not be of great importance because bonds with metals, galvanized and chemically treated as they are in automobile applications, are usually much stronger and more durable than those with other materials such as SMC. Also, adhesive bonds in compression ("negative peel stresses") are much less likely to fail than those in tension unless they are also accompanied by extremely high shear stresses.

For Load Case 2, the symmetry of the shear stress distributions observed for Case 1 is not present. This is most likely because of differences in the manner of the loading. In Case 1, the out-of-plane bending and twisting of the model was due entirely to the stiffening effects of the bonded SMC panel. The loading in Case 2 forced the

model to bend at only one of the vertical steel frame members where higher stresses are indeed found. If allowances are made for these induced higher stresses, a symmetry of the shear stress distributions can be envisioned.

The peel stress distribution exhibits a degree of symmetry for Load Case 2. As in Case 1, the highest stresses are at the steel frame interface and decrease towards the SMC interface. The stresses on the loaded left vertical member are not appreciably higher than those on the unloaded member. The only hint of the location of the loads on the model can be seen as a small area of high compressive stresses at the upper left-hand corner of the adhesive/sealer. Curiously, relatively high compressive stresses appear at all four corners of the model. This phenomena is more evident in the high-modulus adhesive than in the sealer. Again, although the magnitude of the stresses are high, compressive stresses contribute little to the failure of adhesive bonds.

4.0 CONCLUSIONS

The prediction of stresses in adhesively bonded joints has historically been a very difficult task. In many cases, bonded joints were, and still are, designed based upon proven methods without insight into the magnitudes of stresses present in the system. While the method examined here has not been proven infallible, previous efforts have shown some promise in its utility.

Based upon those previous successes, this effort has attempted to shed some light on the kinds of stresses present in a typical automotive joint. Though the accuracy of this work has yet to be verified through experimental methods, some very important qualitative information can be obtained. For example, the peel stresses in the adhesive and sealer layers are extremely low, being less than 4% of its' UTS. This is significant because in similar materials, nonlinear viscoelastic behavior does not manifest itself until stresses reach 20% of UTS. Therefore, it is possible to continue the time dependent analysis of the joint without considering any stress dependency of the adhesive/sealer.

Also, the effect of different loading conditions on the stresses in the adhesive/sealer layer can be studied. It appears that in both the shear load (Load Case 1) and the torsional, warping load (Load Case

2), the adhesive/sealer peel stresses are very similar in magnitude and in trends through the bond thickness.

In the case of the shear stresses, there is a notable difference in magnitude between the adhesive and sealer. In both Load Case 1 and 2, the adhesive shear stresses are an order of magnitude greater than the sealer shear stresses. This difference is consistent through the bond thickness for Load Case 1. For Load Case 2, the shear stresses for the PG-1 adhesive are considerably (relatively) greater at the SMC interface than for the sealer. There is also an interesting difference in trends in shear stress through the bond thickness between Load Case 1 and 2. For Load Case 1, the shear stresses go from negative to positive through the bond thickness (from the frame interface to the SMC interface) while for Load Case 2, the trend is the opposite, going from positive to negative. As stated earlier, this phenomena is due to the direction the frame is forced to bend by each loading condition.

With this kind of information in hand, a better qualitative feel of how to design and what to expect from an adhesively bonded joint may be obtained. Again, this linear elastic analysis did not make any allowances for time dependent effects and later efforts should address such challenges. Further work is currently being done in order to better establish the correlation between experimental data and analytical predictions using simpler joint geometries such as the single lap shear joint and thick adherend joints.

REFERENCES

1. Alkonis, J. J., W. J. MacKnight, M. C. Shen, Introduction to Polymer Viscoelasticity, John Wiley & Sons, New York, 1972
2. Cooper, J. N., "The Effect of Thermal Stresses on the Viscoelastic Behavior of Adhesively Bonded Joints," VPI & SU, September 1987
3. Dillard, D. A., D. H. Morris, H. F. Brinson, "Creep and Creep Rupture of Laminated Graphite/Epoxy Composites," VPI & SU, March 1981
4. Ferry, J. D., Viscoelastic Properties of Polymers, 3rd edition, John Wiley & Sons, New York, 1980
5. Findley, W. N., G. Khosla, "Application of the Superposition Principle and Theories of Mechanical Equations of State, Strain, and Time Hardening to Creep of Plastics Under Changing Loads," Journal of Applied Physics, Vol. 26, No. 7, 1955
6. Findley, W. N., J. S. Y. Lai, "A Modified Superposition Principle Applied to Creep of Nonlinear Viscoelastic Material Under Abrupt Changes in State of Combined Stress," Transactions of the Society of Rheology, Vol. 11, No. 3, 1967
7. Flügge, W., Viscoelasticity, 2nd edition, Springer-Verlag, New York, 1975

8. Gramoll, K. C., D. A. Dillard, H. F. Brinson, "Thermoviscoelastic Characterization and Prediction of Kevlar/Epoxy Composite Laminates," VPI & SU, May 1988
9. Green, A. E., R. S. Rivlin, "The Mechanics of Nonlinear Materials with Memory," Arch. Rational Mech. Anal., Vol. 1, No. 1, pp. 1-21, 1957
10. Kohl, W. S., "Analysis and Modelling of Creep Behavior in Viscoelastic Adhesives," Unpublished, 1990
11. Minford, J. D., "Adhesives," Durability of Structural Adhesives, A. J. Kinloch, Ed., pp.135-214, Applied Science Publishers, 1983
12. Osiroff, T., "Analysis of a Bonded Joint Using Bulk Adhesive Properties," VPI & SU, December 1988
13. Phillips, P. G., "Adhesives, Sealants in Autos to Grow at 250% of GNP," Adhesives Age, August 1989
14. Post, D., R. Czarnek, J. D. Wood, D. Joh, "Deformations and Strains in a Thick Adherend Lap Joint," Adhesively Bonded Joints: Testing, Analysis, and Design, ASTM STP 981, W. S. Johnson, Ed., American Society for Testing and Materials, pp. 107-118, Philadelphia, 1988
15. Reddy, J. N., An Introduction to the Finite Element Method, McGraw Hill, 1984
16. Schapery, R. A., "On the Characterization of Nonlinear Viscoelastic Materials," Polymer Engineering and Science, Vol. 9, No.4, 1969

17. Tuttle, M. E., H. F. Brinson, "Accelerated Viscoelastic Characterization of T300/5208 Graphite-Epoxy Laminates," VPI & SU, March 1984

APPENDIX: A

The following figures are of the automobile joint model analyzed in this work:

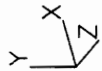
1. Finite element mesh of joint; “front view”
2. Finite element mesh of joint; “back view”
3. Close-up view of elements through thickness of joint

Database: model2
View : No stored View
Task: Mesh Creation
Model: I-FE MODEL1

Units : SI
Display : No stored Option
Model Bin: I-MAIN
Associated Workset: I-WORKING SET1

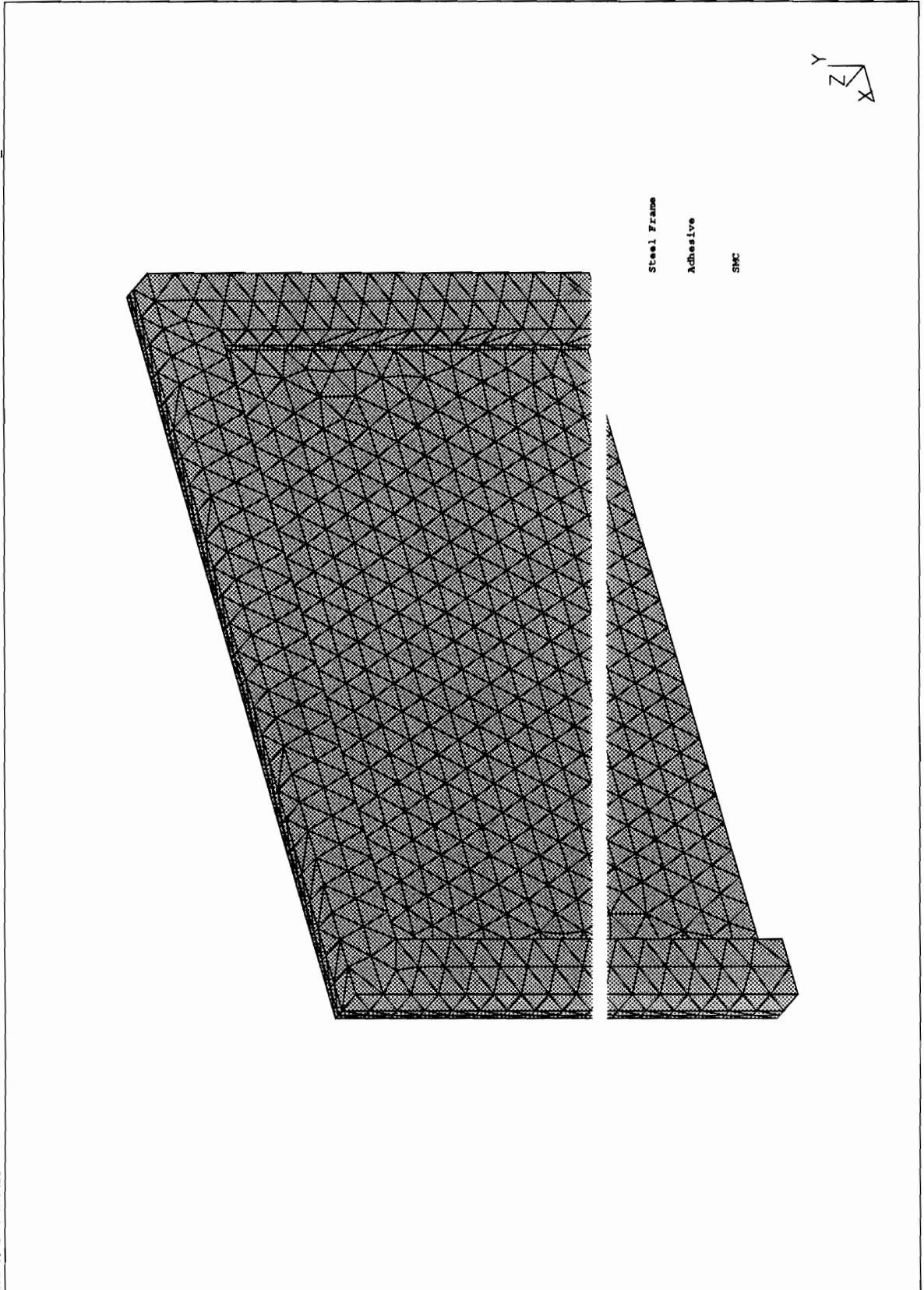


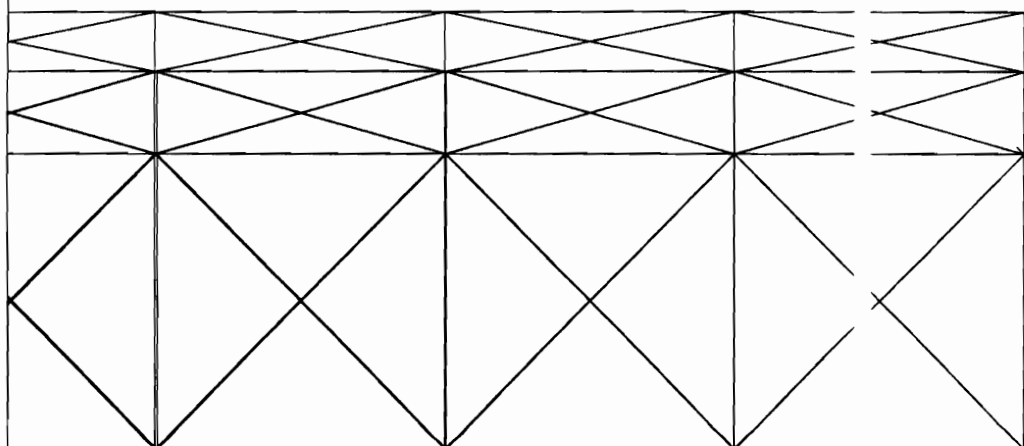
Steel Frame
Adhesive
SMC



Database: model2
View : No stored View
Task: Mesh Creation
Model: 1-FE MODEL1

Units : SI
Display : No stored Option
Model Bin: 1-MAIN
Associated Workset: 1-WORKING_SET1



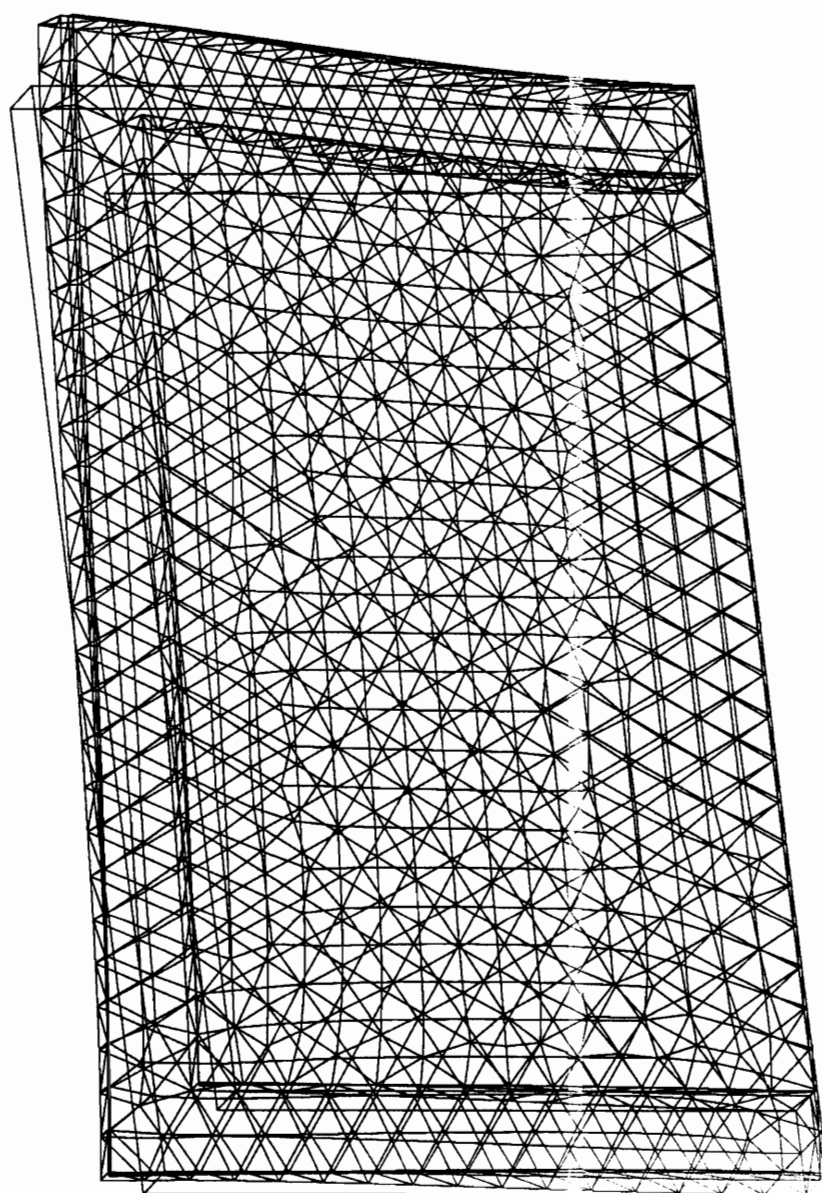


APPENDIX: B

3-dimenisonal views of deformed mesh.

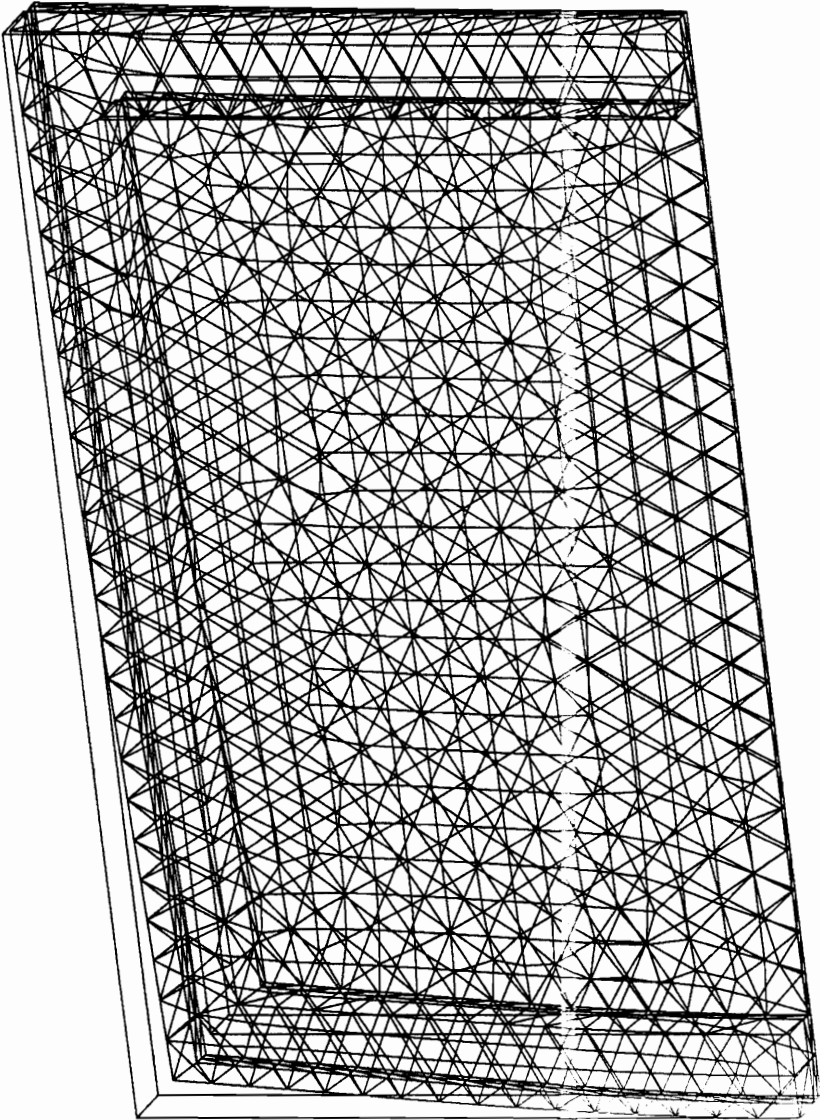
1. Deformation due to Load Case 1; “Shear Loading”
2. Deformation due to Load Case 2; “Warp Loading”

ABAQUS 4-8-4 : *STATIC, DIRECT



SDRC I-DEAS V: FE_Modeling_&Analysis

ABAQUS 4-8-4 : *STATIC, DIRECT
LOADCASE:1 TIMESTEP:1 TIME: 1.0
DISPLACEMENT - MAG MIN: 0.00 MAX: 0.000858



APPENDIX: C

Note: The analysis was done in SI units and therefore, all stresses in the plots are in Pascals unless otherwise noted.

There are 24 plots: For each loading condition (Load Case 1 & 2), there are 12 plots, i.e. 6 plots for each adhesive/sealer (PG-1 & generic sealer). Each set of 6 plots includes 3 shear stress plots and 3 peel stress plots. Those 3 plots are made at three different cutting planes of the adhesive/sealer layer, e.g. adhesive/frame interface, middle adhesive layer, adhesive/SMC interface.

The plots can be identified in the following way:

1. Material and Load Case is identified in the upper left-hand corner of the main heading labelled, "Database."
2. Stress component is shown on the bottom left-hand side of the plot heading. It is labelled "STRESS - XY," for shear stress and "STRESS - Z," for peel stress.
3. The location of the cutting-plane of the plot is shown above the color bar legend on the right-hand side of the plot.

Plots are organized in the following repeating order:

Load Case 1: PG-1 Adhesive:

Adhesive/Frame Interface:

Shear Stress

Peel Stress

Middle Adhesive:

Shear Stress

Peel Stress

Adhesive/SMC Interface:

Shear Stress

Peel Stress

Load Case 2: PG-1 Adhesive:

(repeat above sequence)

Load Case 1: Sealer:

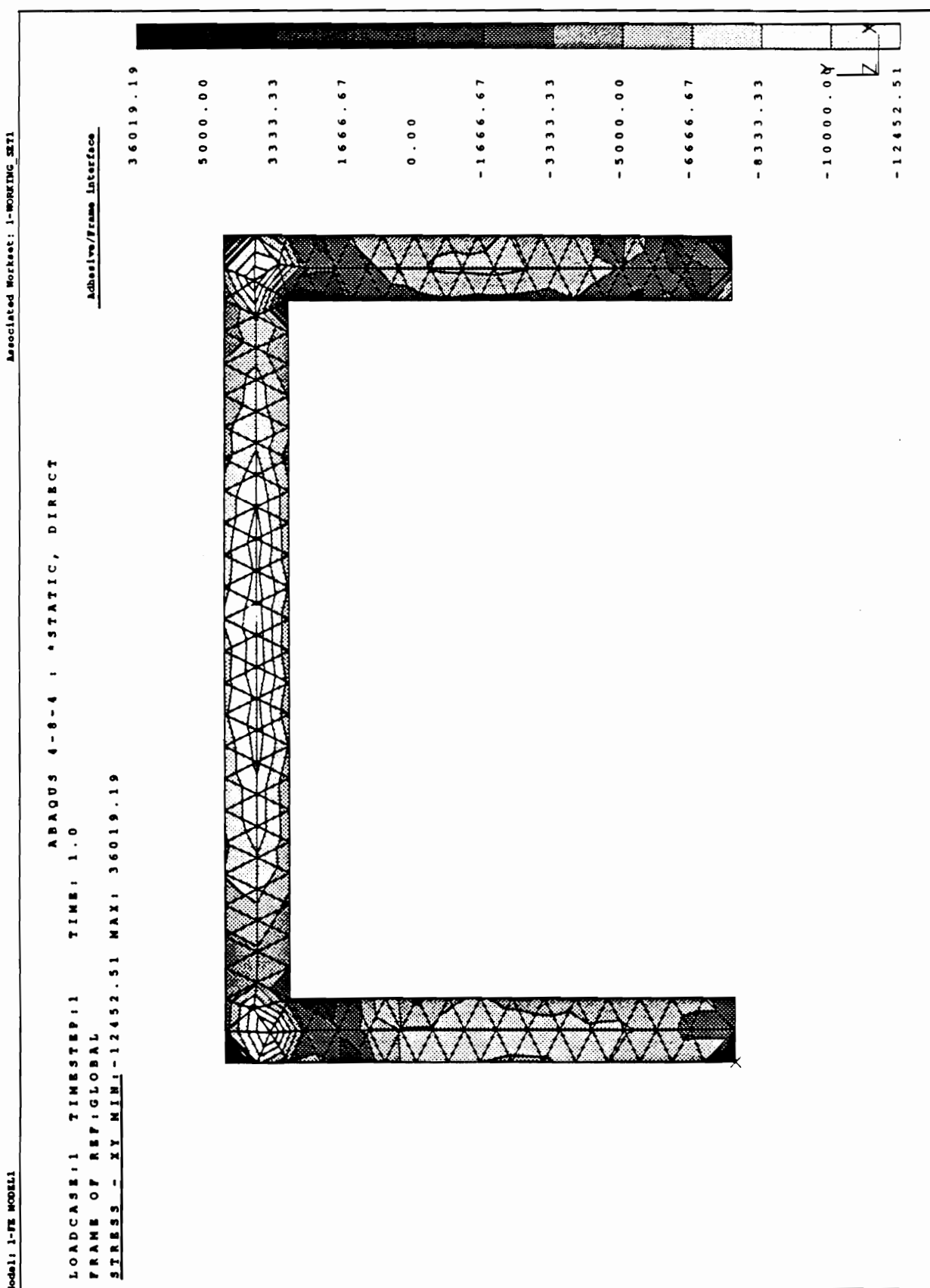
(repeat above sequence)

Load Case 2: Sealer:

(repeat above sequence)

Database: Adhesive E-55kel Shear
View : No stored View
Task: Post Processing
Model: 1-FE MODEL1

Display : No stored Option
Model Bin: 1-MAX
Associated Worksheet: 1-WORKING SHEET



Database: Adhesive E-55kai Shear
View : No stored View
Task: Post Processing
Model: 1-FE MODEL1

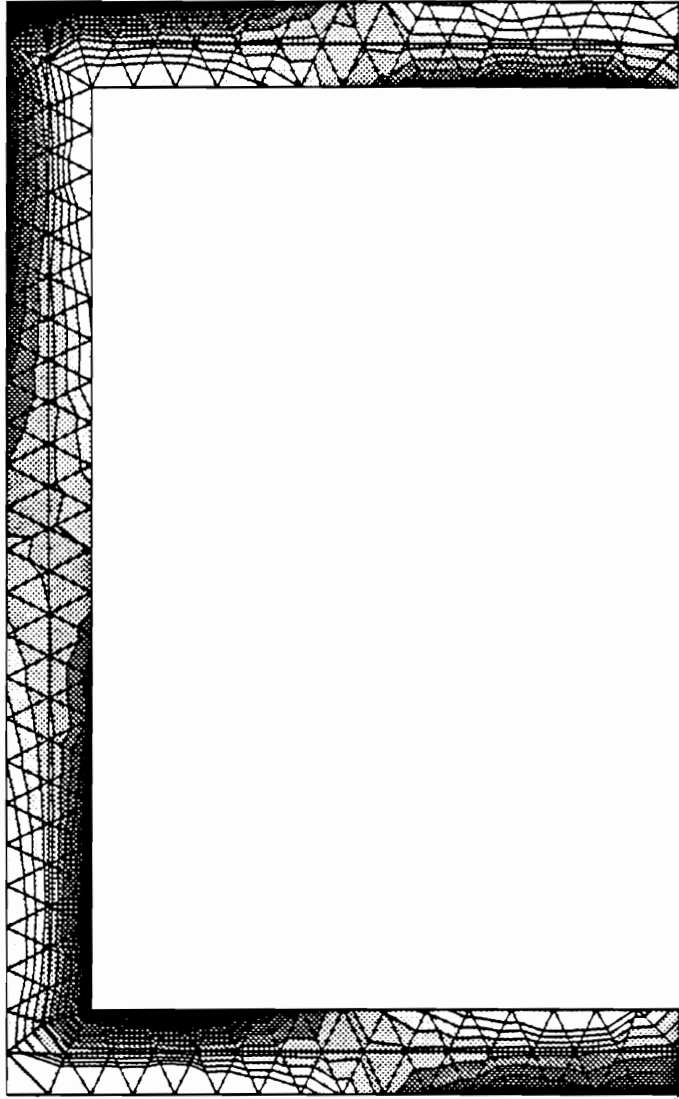
Units : SI
Display : No stored Option
Model Bin: 1-MAIN
Associated Worksheet: 1-WORKING_SXT1

ABAQUS 4-8-4 : *STATIC, DIRECT

LOADCASE:1 TIMESTEP:1 TIME: 1.0
FRAME OF REF:GLOBAL
STRESS - Z MIN:-4.05E+05 MAX: 3.39E+05

Adhesive/Frame Interface

3.39E+05
1.40E+05
1.17E+05
93333.34
70000.00
46666.67
23333.34
0.00
-23333.33
-46666.67
-70000.00
-4.05E+05



Database: Adhesive E-51kral Shear
View : No stored View
Task: Post Processing
Model: 1-FE MODEL1

Units : SI
Display : No stored Option
Model Bin: 1-MAIN
Associated Worksheet: 1-WORKING_SXT1

ABAQUS 4-8-4 : *STATIC, DIRECT

LOADCASE:1 TIMESTEP:1 TIME: 1.0
FRAME OF REF:GLOBAL
STRESS - XY MIN:-12452.51 MAX: 36019.19

Middle Adhesive

36019.19
10000.00
7777.78
5555.56
3333.33
1111.11
-1111.11
-3333.33
-5555.56
-7777.78
-10000.00
-12452.51



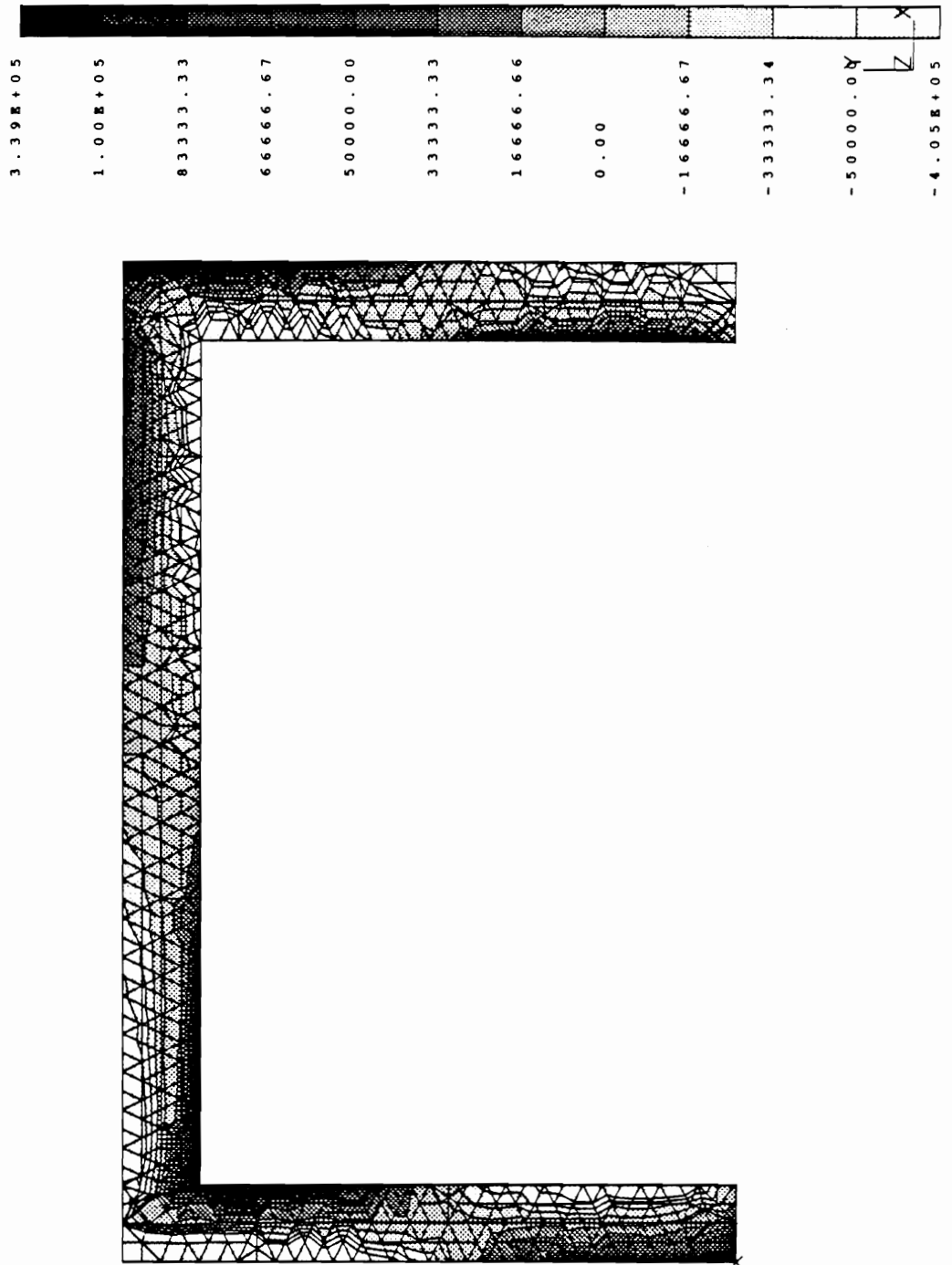
Database: Adhesive E-55ksi Shear
View : No stored View
Task: Post Processing
Model: 1-FE MODEL1

Units : SI
Display : No stored Option
Model Bin: 1-MAIN
Associated Worksheet: 1-WORKING SET1

ABAQUS 4-8-4 : *STATIC, DIRECT

LOADCASE:1 TIMESTEP:1 TIME: 1.0
FRAME OF REF:GLOBAL
STRESS - Z MIN:-4.05E+05 MAX: 3.39E+05

Middle Adhesive



Database: Adhesive E-55kai Shear
View : No stored View
Task: Post Processing
Model: 1-FE MODEL1

Units : SI
Display : No stored Option
Model Bln: 1-MAIN
Associated Worksheet: 1-WORKING SET1

ABAQUS 4-8-4 : *STATIC, DIRECT

LOADCASE:1 TIMESTEP:1 TIME: 1.0
FRAME OF REF: GLOBAL
STRESS - XY MIN: -12452.51 MAX: 36019.19

Adhesive/SMC Interface

36019.19

20000.00

17222.22

14444.45

11666.67

8888.89

6111.11

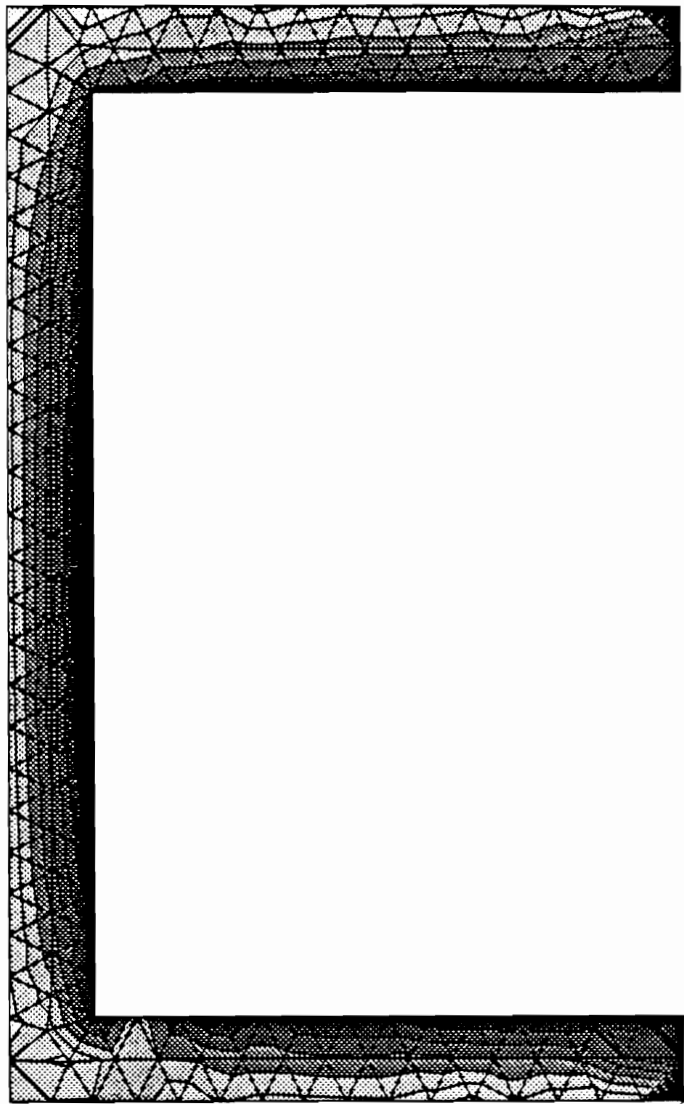
3333.33

555.56

-2222.22

-5000.00 Y

-12452.51



Database: Adhesive E-53kel Shear

View : No stored View

Task: Post Processing

Model: 1-FE MODEL1

Units : SI

Display : No stored Option

Model Bin: 1-MAIN

Associated Worksheet: 1-WORKING.SET1

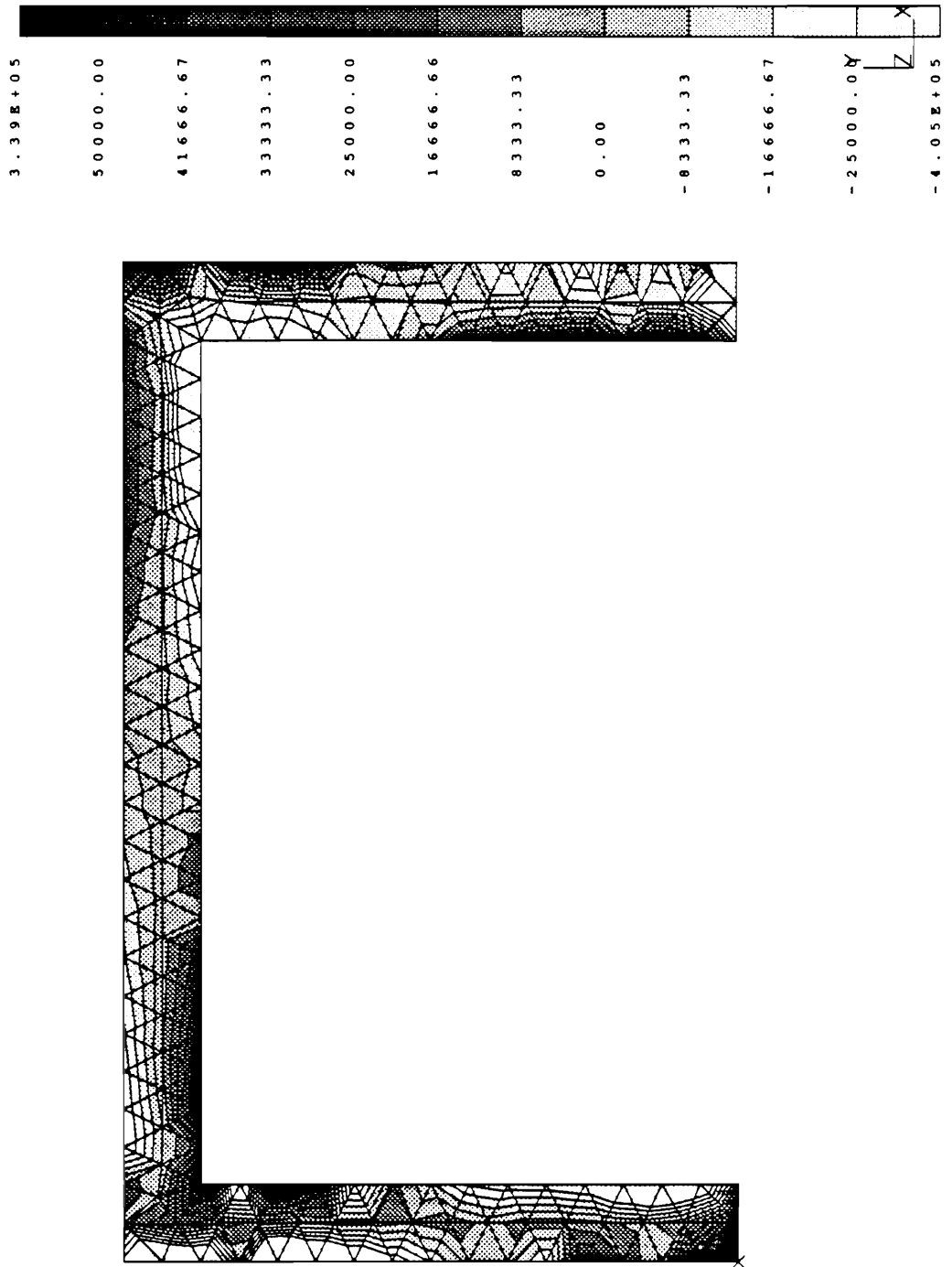
ABAQUS 4-8-4 : *STATIC, DIRECT

LOADCASE:1 TIMESTEP:1 TIME: 1.0

FRAME OF REF:GLOBAL

STRESS - Z MIN:-4.05E+05 MAX: 3.39E+05

Adhesive/SNC Interface



Database: Adhesive E-55ksi Torsion

View : No stored View

Task: Post Processing

Model: 1-FE MODEL1

Units : SI

Display : No stored Option

Model Bln: 1-MAIN

Associated Workset: 1-WORKING SET1

ABAQUS 4-8-4 : *STATIC, DIRECT

LOADCASE:1 TIMESTEP:1 TIME: 1.0

FRAME OF REF:GLOBAL

STRESS - XY MIN:-38403.83 MAX: 36508.19

Adhesive/Frame Interface

36508.19

30000.00

25000.00

20000.00

15000.00

10000.00

5000.00

0.00

-5000.00

-10000.00

-15000.00

-38403.83

Database: Adhesive E-55ksi Torsion
View : No stored View
Task: Post Processing
Model: 1-FE MODEL1

Units : SI
Display : No stored Option
Model Bln: 1-MAIN
Associated Worksheet: 1-WORKING SET1

ABAQUS 4-8-4 : *STATIC, DIRECT

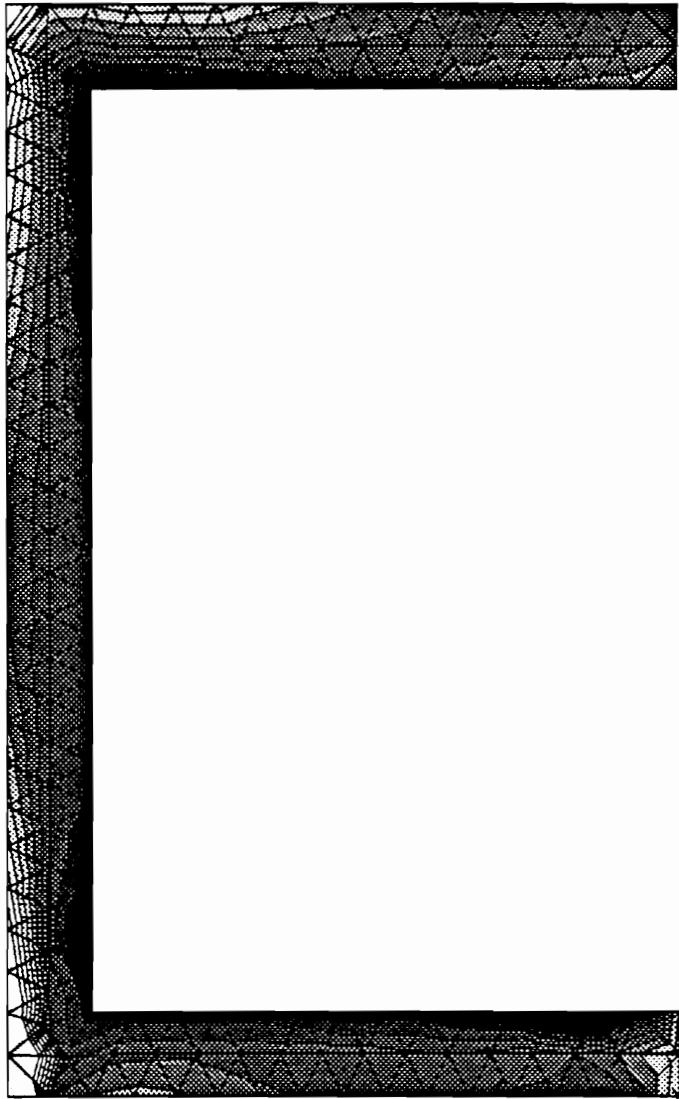
LOADCASE:1 TIMESTEP:1 TIME: 1.0

FRAME OF REF:GLOBAL

STRESS - 2 MIN:-7.53E+05 MAX: 3.45E+05

Adhesive/Frame Interface

3.45E+05
1.25E+05
83333.35
41666.69
0.015625
-41666.66
-83333.33
-1.25E+05
-1.67E+05
-2.08E+05
-2.50E+05
-7.53E+05



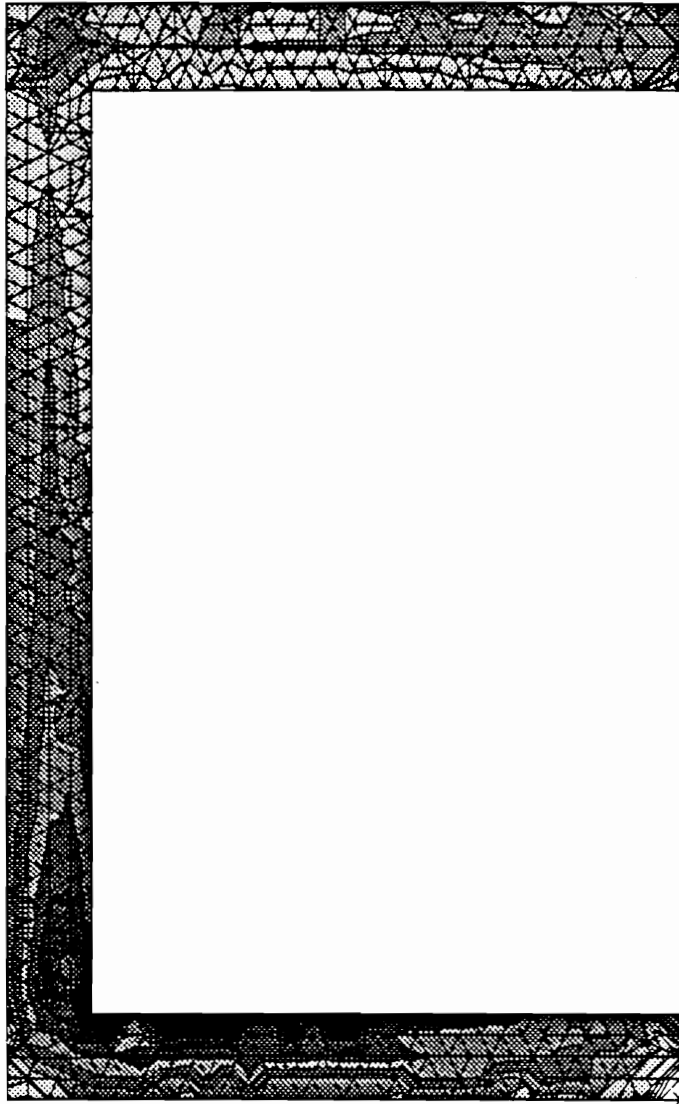
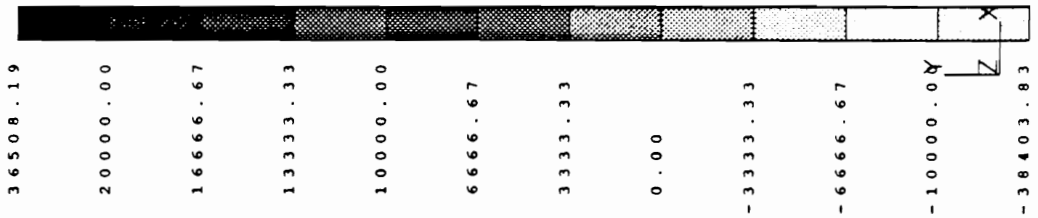
Database: Adhesive E-55kai Torsion
View : No stored View
Task: Post Processing
Model: 1-FE MODEL1

Units : SI
Display : No stored Option
Model Bin: 1-MAIN
Associated Worksheet: 1-WORKING SET1

ABAQUS 4-8-4 : *STATIC, DIRECT

LOADCASE:1 TIMESTEP:1 TIME: 1.0
FRAME OF REF:GLOBAL
STRESS - XY MIN:-38403.83 MAX: 36508.19

Middle Adhesive



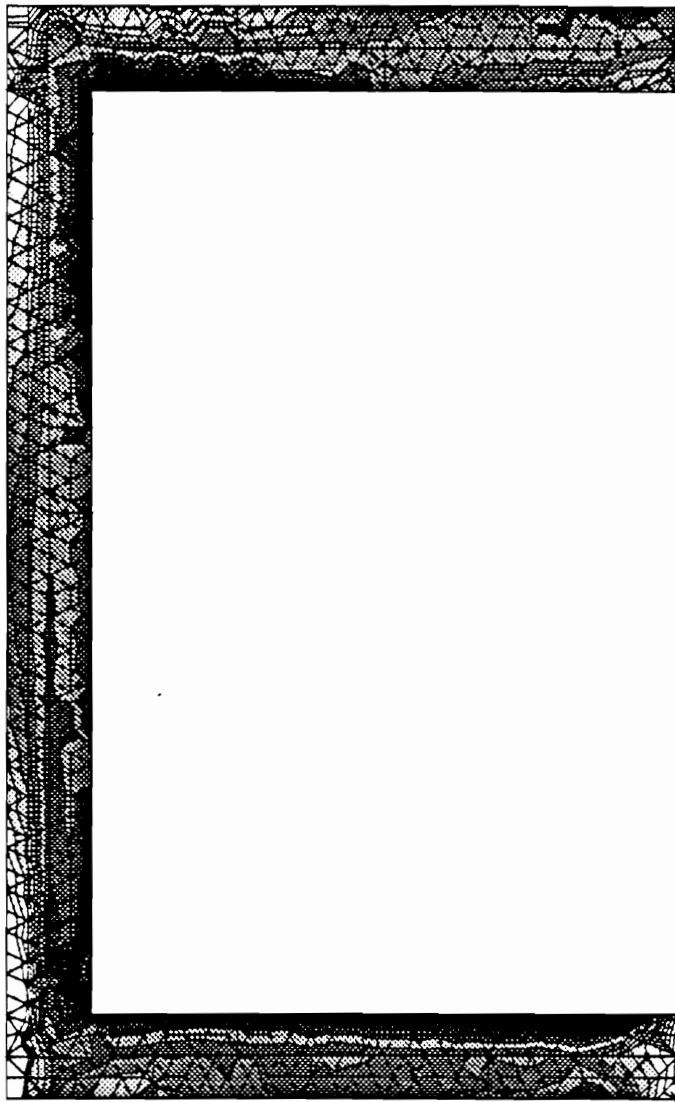
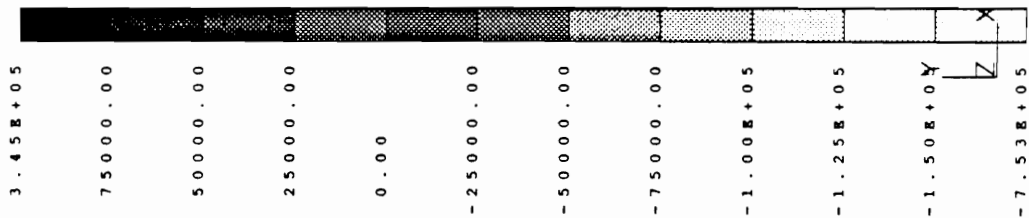
Database: Adhesive E-55ke1 Torsion
View : No stored View
Task: Post Processing
Model: 1-FE MODEL1

Units : SI
Display : No stored Option
Model Bin: 1-MATH
Associated Worksheet: 1-WORKING_XYT1

ABAQUS 4-8-4 : *STATIC, DIRECT

LOADCASE:1 TIMESTEP:1 TIME: 1.0
FRAME OF REF: GLOBAL
STRESS - 2 MIN:-7.53E+05 MAX: 3.45E+05

Middle Adhesive



Database: Adhesive E-55ksi Torsion

View : No stored View

Task: Post Processing

Model: 1-FE MODEL1

Units : SI

Display : No stored Option

Model Bin: 1-MAIN

Associated Worksheet: 1-WORKING_SMT1

ABAQUS 4-8-4 : *STATIC, DIRECT

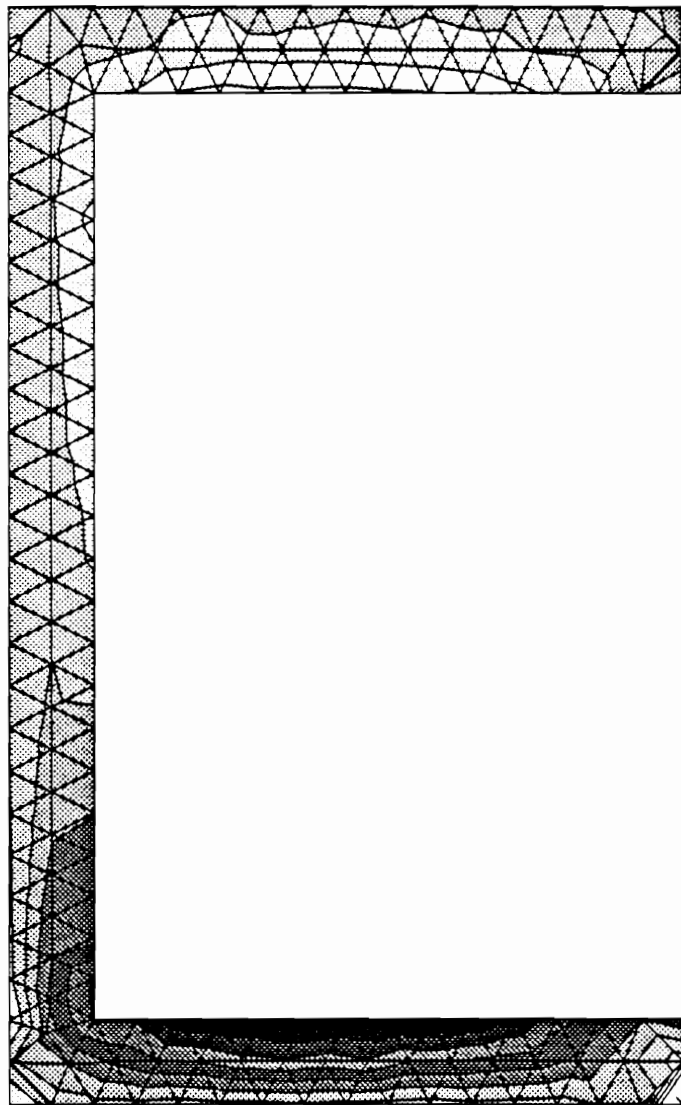
LOADCASE:1 TIMESTEP:1 TIME: 1.0

FRAME OF REF: GLOBAL

STRESS - XY MIN: -38403.83 MAX: 36508.19

Adhesive/SMC Interface

36508.19
30000.00
25000.00
20000.00
15000.00
10000.00
5000.00
0.00
-5000.00
-10000.00
-15000.00
-38403.83



Database: Adhesive E-55ksi Torsion
View : No stored View
Task: Post Processing
Model: 1-FE MODEL1

Units : SI
Display : No stored Option
Model Bin: 1-MAIN
Associated Worksheet: 1-WORKING SET1

ABAQUS 4-8-4 : *STATIC, DIRECT

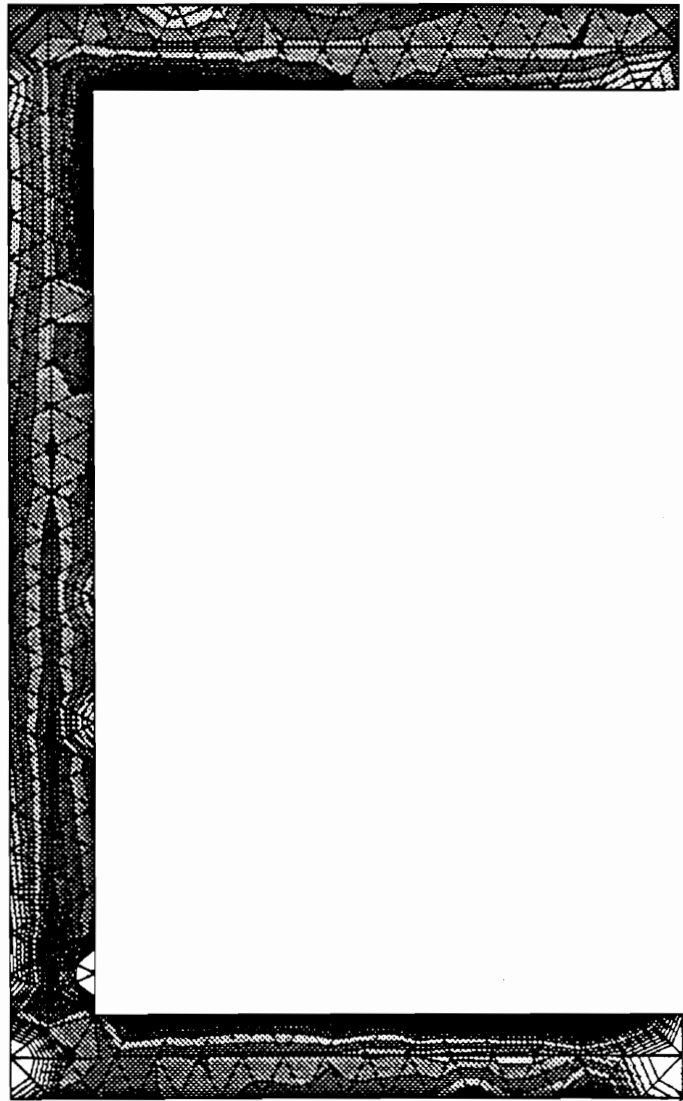
LOADCASE:1 TIMESTEP:1 TIME: 1.0

FRAME OF REF:GLOBAL

STRESS - Z MIN:-7.53E+05 MAX: 3.45E+05

Adhesive/SWC Interface

3.45E+05
50000.00
33333.33
16666.66
0.00
-16666.67
-33333.34
-50000.00
-66666.67
-83333.34
-1.00E+05
-7.53E+05

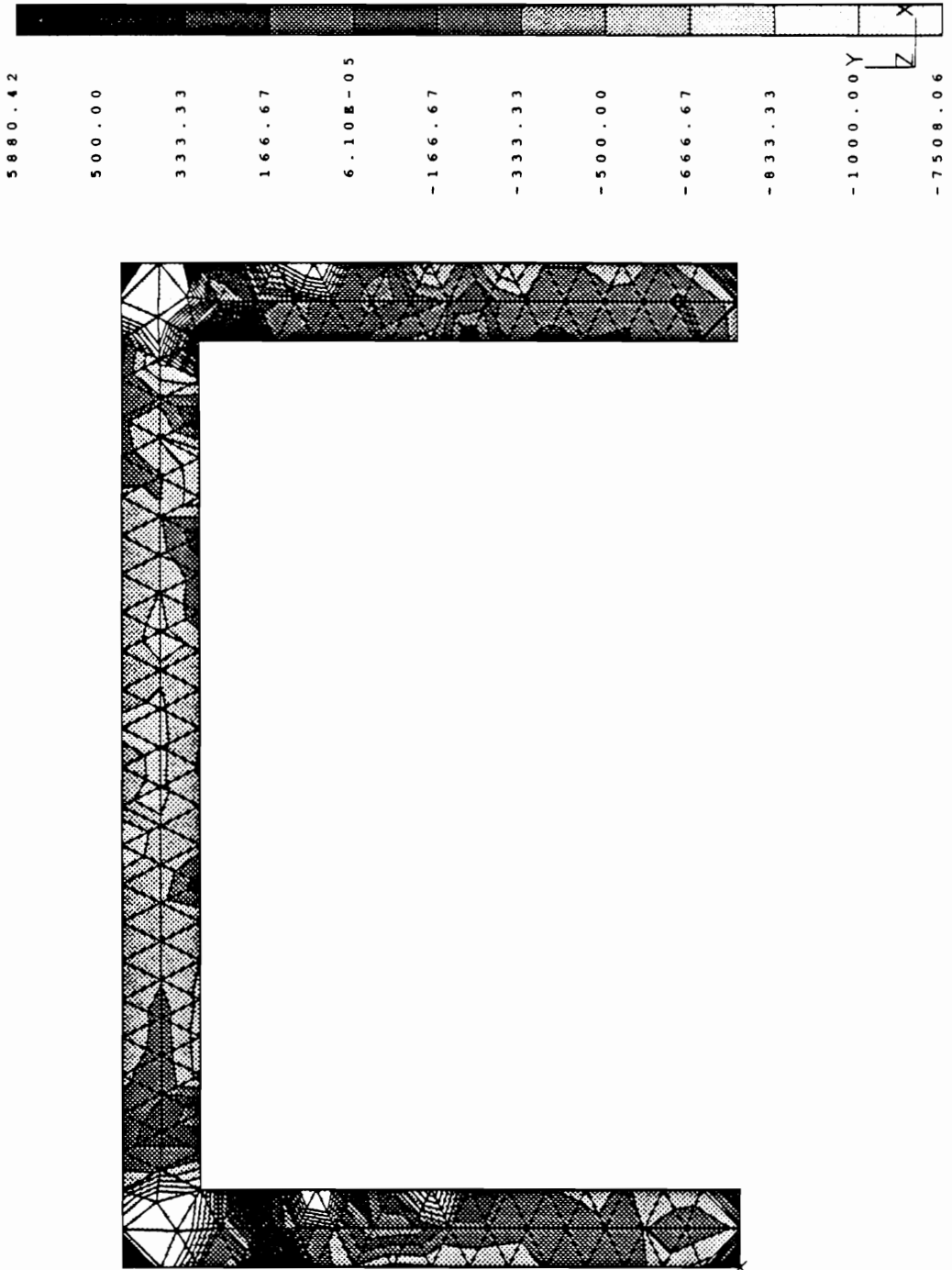


Database: Sessler E-5kel Shear
View : No stored View
Task: Post Processing
Model: 1-FE MODEL1

Units : SI
Display : No stored Option
Model Bin: 1-MAIN
Associated Worksheet: 1-WORKING SET1

ABAQUS 4-8-4 : *STATIC, DIRECT

LOADCASE:1 TIMESTEP:1 TIME: 1.0
FRAME OF REF:GLOBAL
STRESS - XY MIN:-7508.06 MAX: 5880.42



Database: Sealer E-Skal Shear
View : No stored View
Task: Post Processing
Model: 1-FE MODEL1

Display : No stored Option
Model Bin: 1-MAIN
Associated Worksheet: 1-WORKING_SHEET1

Units : SI

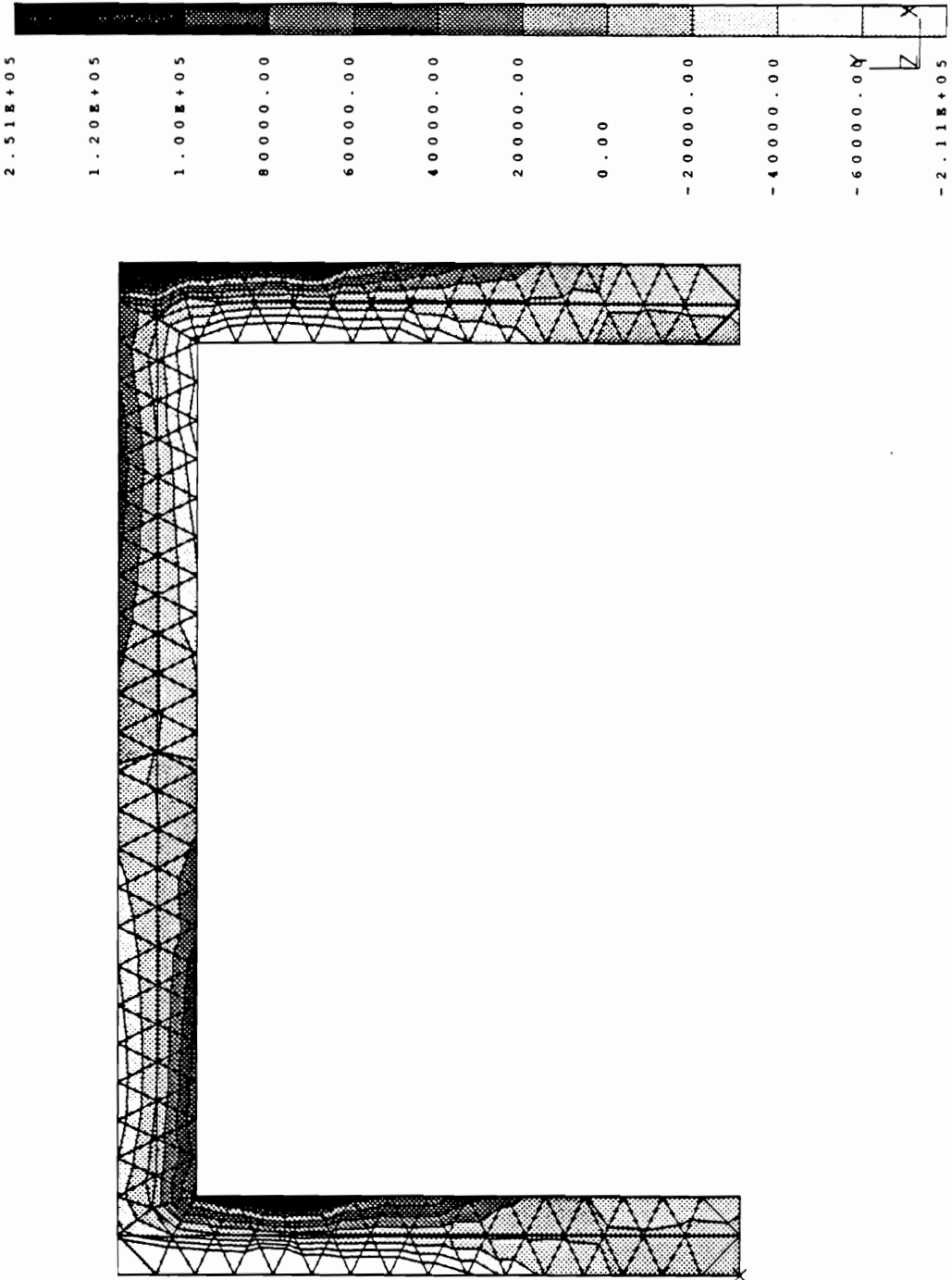
ABAQUS 4-8-4 : *STATIC, DIRECT

LOADCASE:1 TIMESTEP:1 TIME: 1.0

FRAME OF REF:GLOBAL

STRESS - Z MIN:-2.11E+05 MAX: 2.51E+05

Sealer/Frame Interface



Database: Sealer E-5kel Shear
View : No stored View
Task: Post Processing
Model: 1-FE MODEL1

Units : SI
Display : No stored Option
Model Bin: 1-MAIN
Associated Worksheet: 1-WORKING SET1

ABAQUS 4-8-4 : *STATIC, DIRECT

TIME: 1.0

LOADCASE:1 TIMESTEP:1

FRAME OF REF:GLOBAL

STRESS - XY MIN:-7508.06 MAX: 5880.42

Middle Sealer

5880.42

1000.00

833.33

666.67

500.00

333.33

166.67

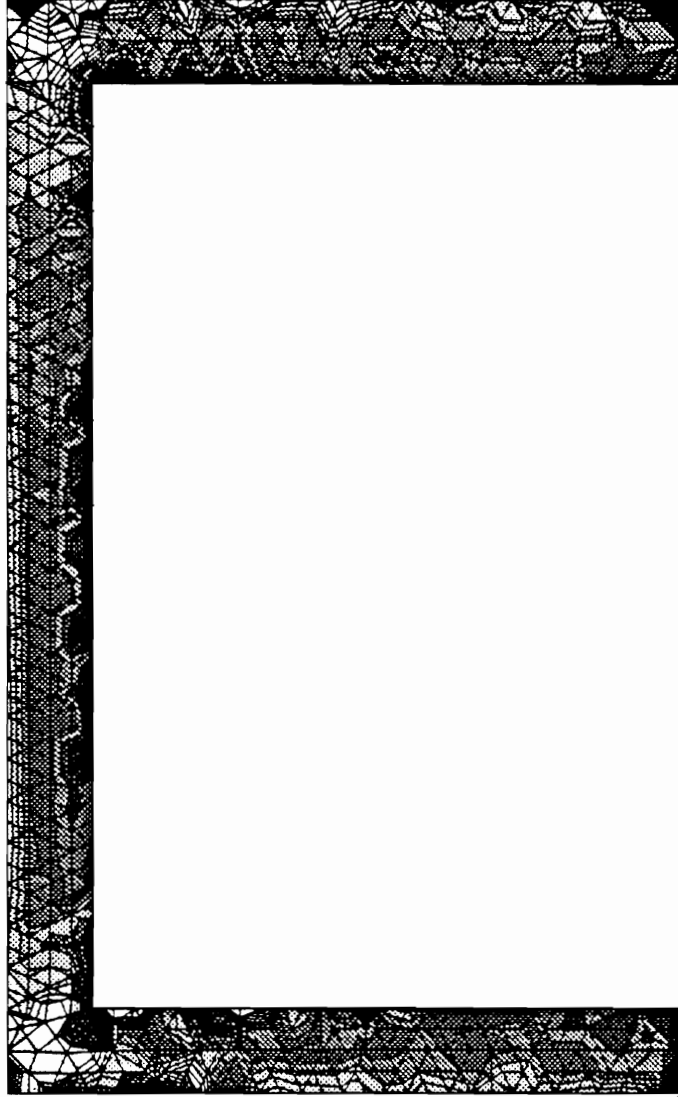
3.05E-05

-166.67

-333.33

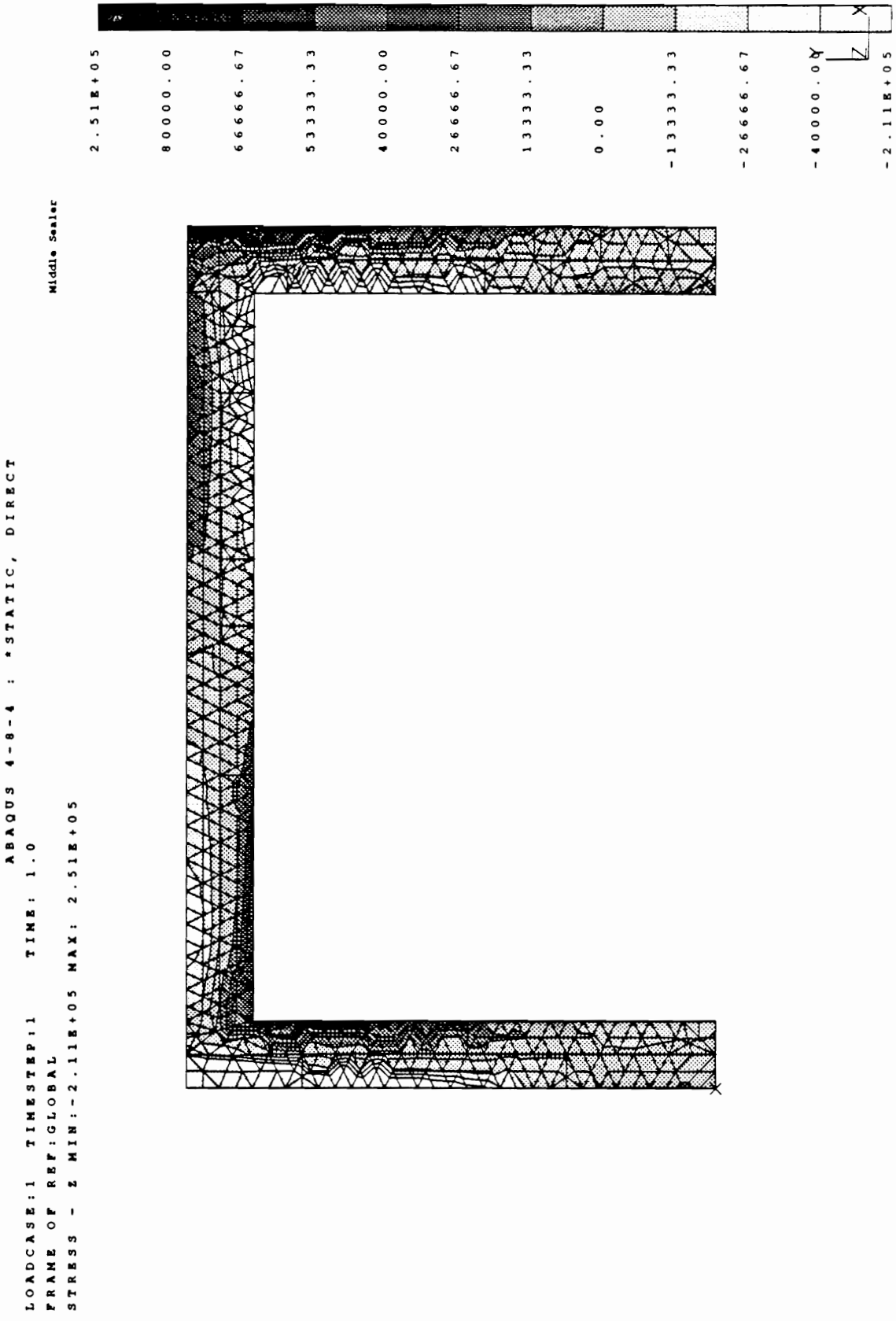
-500.00

-7508.06



Database: Sealer E-5ksi Shear
View : No stored View
Task: Post Processing
Model: 1-FE MODEL1

Units : SI
Display : No stored Option
Model Bin: 1-MAIN
Associated Worksheet: 1-WORKING.SMT1



Database: Sealer E-Skel Shear
View : No stored View
Task: Post Processing
Model: 1-FE MODEL1

Display : No stored Option
Model Bin: 1-MAIN
Associated Worksheet: 1-WORKING_SET1

Units : SI

ABAQUS 4-8-4 : *STATIC, DIRECT

LOADCASE:1 TIMESTEP:1 TIME: 1.0

FRAME OF REF:GLOBAL

STRESS - XY MIN:-7508.06 MAX: 5880.42

Sealer/SMC Interface

5880.42

2000.00

1666.67

1333.33

1000.00

666.67

333.33

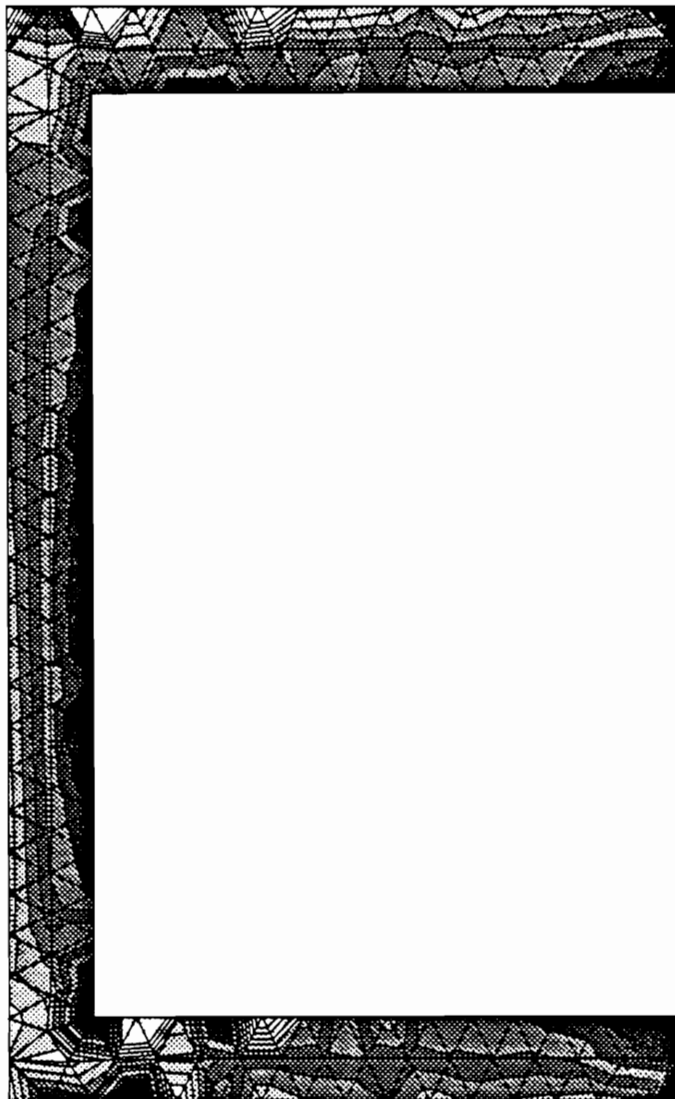
6.10E-05

-333.33

-666.67

-1000.00Y

-7508.06



Database: Sealer E-Skel Shear
View : No stored View
Task: Post Processing
Model: 1-FE MODEL1

Display : No stored Option
Model Bin: 1-MAIN
Associated Worksheet: 1-WORKING_SKT1
Units : SI

ABAQUS 4-8-4 : *STATIC, DIRECT

TIME: 1.0

LOADCASE:1 TIMESTEP:1

FRAME OF REF:GLOBAL

STRESS - 2 MIN:-2.11E+05 MAX: 2.51E+05

Sealer/SWC Interface

2.51E+05

40000.00

33333.33

26666.67

20000.00

13333.33

6666.67

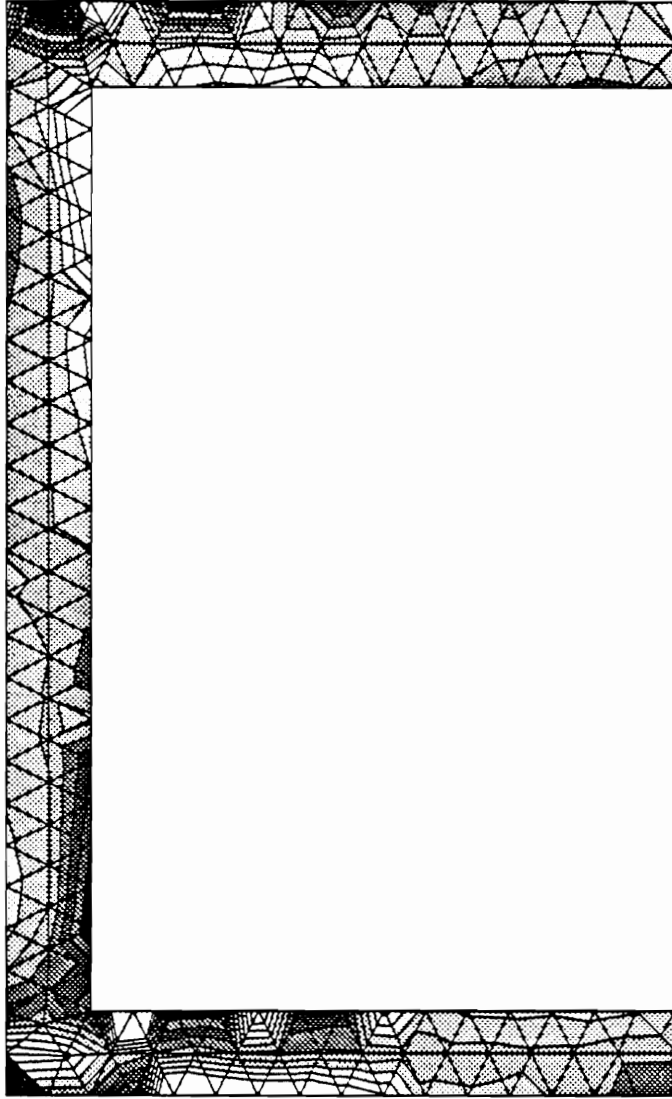
0.00

-6666.67

-13333.33

-20000.00

-2.11E+05



Database: Sealer E-Skel Torsion
View : No stored View
Task: Post Processing
Model: I-FE MODEL1

Units : SI
Display : No stored Option
Model Bin: I-MAIN
Associated Worksheet: I-WORKING_SMT1

ABAQUS 4-8-4 : *STATIC, DIRECT

LOADCASE:1 TIMESTEP:1 TIME: 1.0
FRAME OF REF:GLOBAL
STRESS - XY MIN:-8828.14 MAX: 7418.03

Sealer/Frame Interface

7418.03

3000.00

2500.00

2000.00

1500.00

1000.00

500.00

0.00

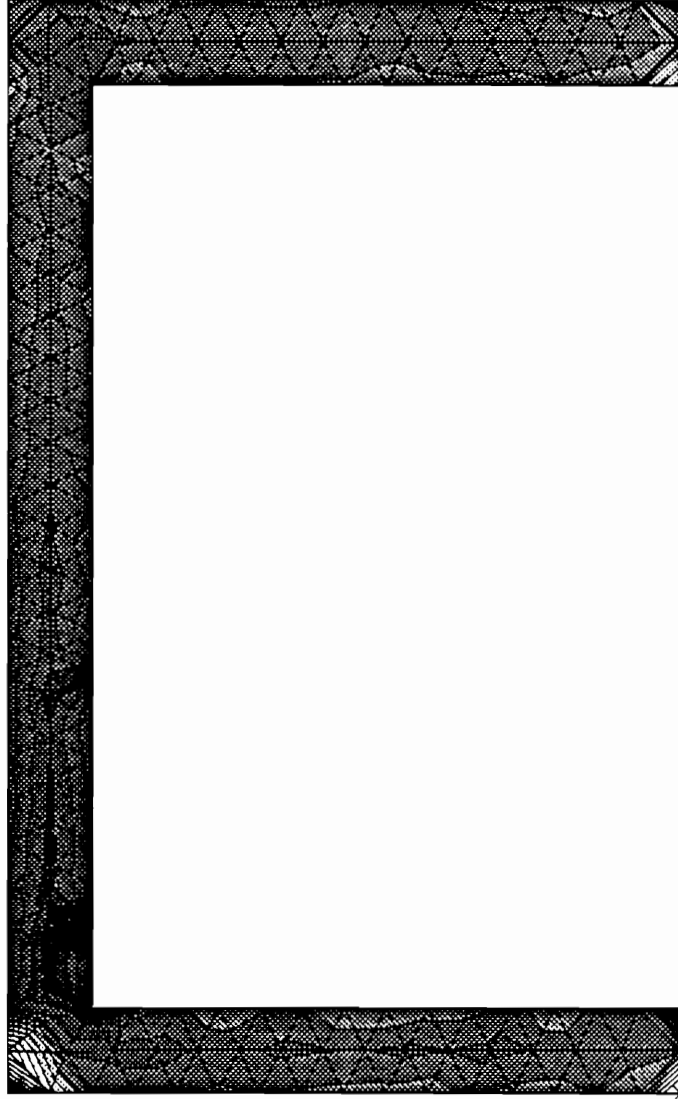
-500.00

-1000.00

-1500.00 Y

Z

-8828.14



Database: Sealer 8-Skel Torsion
View : No stored View
Task: Post Processing
Model: 1-FE MODEL1

Display : No stored Option
Model Bin: 1-MAIN
Associated Worksheet: 1-WORKING.SET1
Units : SI

ABAQUS 4-8-4 : *STATIC, DIRECT

LOADCASE:1 TIMESTEP:1 TIME: 1.0
FRAME OF REF:GLOBAL
STRESS - Z MIN:-2.92E+05 MAX: 1.62E+05

Sealer/Frame Interface

1.62E+05

70000.00

46666.67

23333.33

0.00

-23333.33

-46666.67

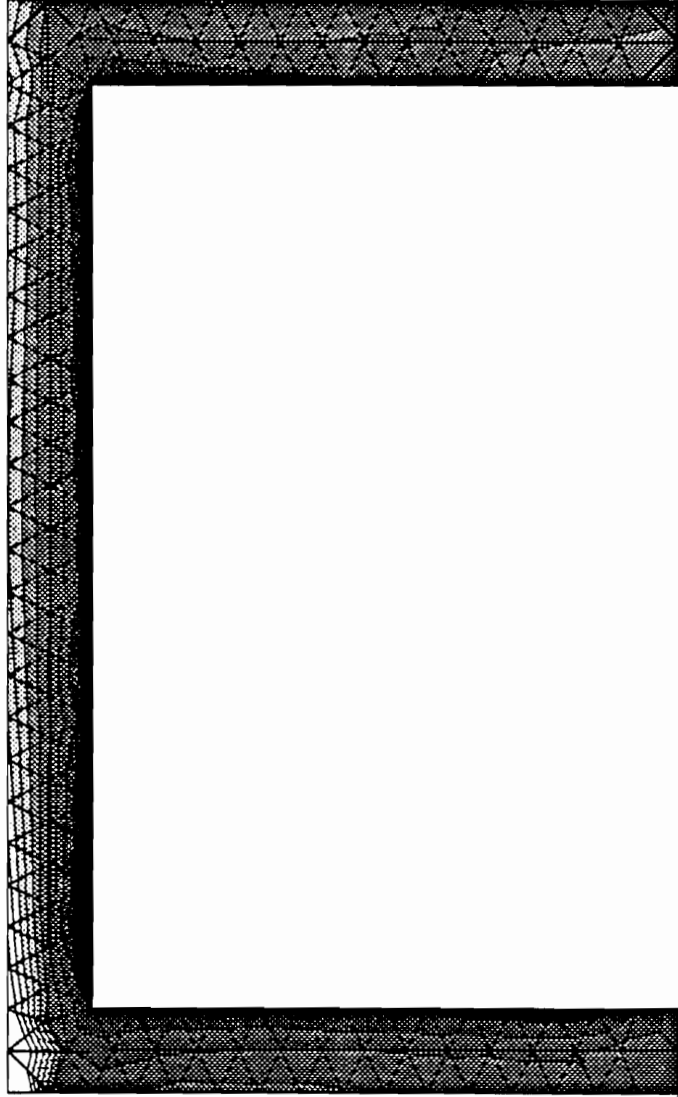
-70000.00

-93333.34

-1.17E+05

-1.40E+05

-2.92E+05



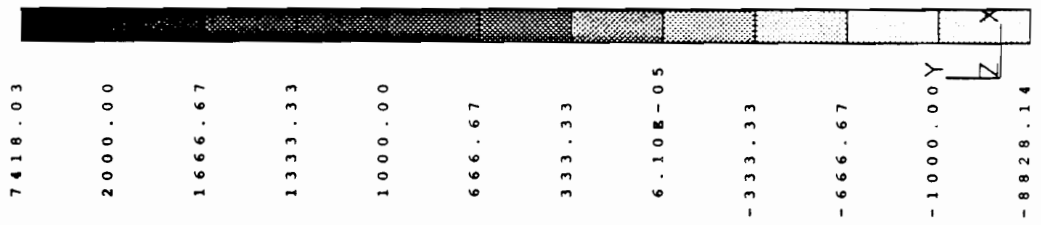
Database: Sealer E-Skel Torsion
View : No stored View
Task: Post Processing
Model: I-FE MODEL1

Units : SI
Display : No stored Option
Model Bin: I-MAIN
Associated Worksheet: I-WORKING.SET1

ABAQUS 4-8-4 : *STATIC, DIRECT

LOADCASE:1 TIMESTEP:1 TIME: 1.0
FRAME OF REF:GLOBAL
STRESS - XY MIN:-8828.14 MAX: 7418.03

Middle Sealer



Database: Sealer E-Skel Torsion
View : No stored View
Task: Post Processing
Model: 1-FE MODEL1

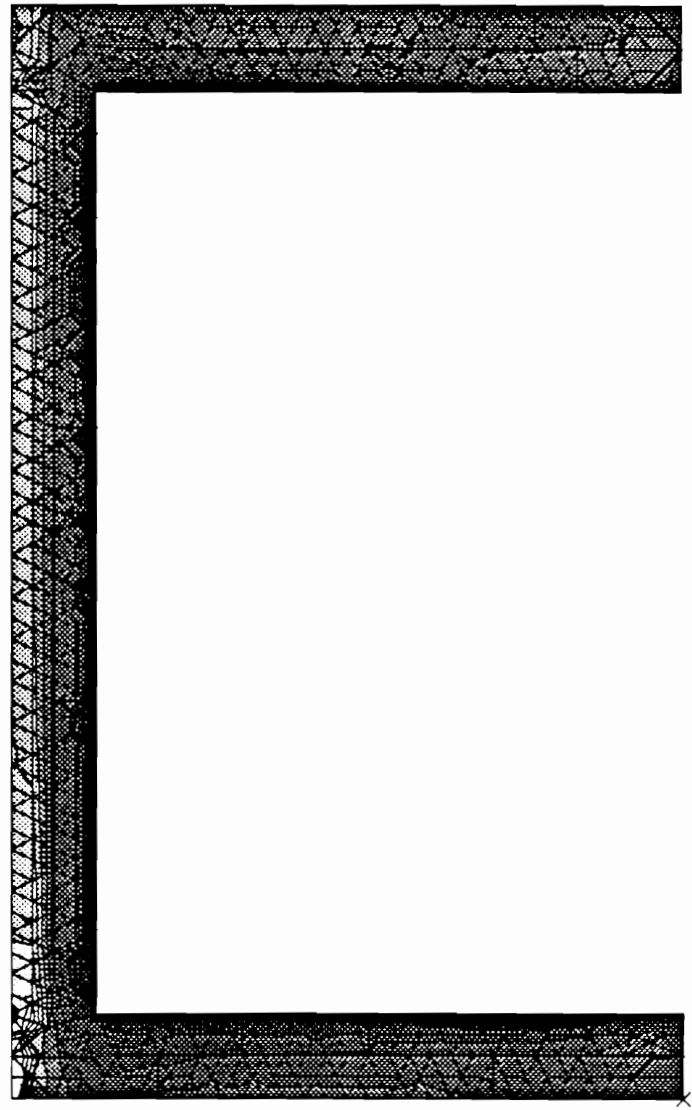
Units : SI
Display : No stored Option
Model Bin: 1-MAIN
Associated Worksheet: 1-WORKING SET1

ABAQUS 4-8-4 : *STATIC, DIRECT

LOADCASE:1 TIMESTEP:1 TIME: 1.0
FRAME OF REF:GLOBAL
STRESS - X MIN:-2.92E+05 MAX: 1.62E+05

Middle Sealer

1.62E+05
50000.00
33333.33
16666.66
0.00
-16666.67
-33333.34
-50000.00
-66666.67
-83333.34
-1.00E+05
-2.92E+05



Database: Sealer E-Shel Torsion
View : No stored View
Task: Post Processing
Model: 1-FE MODEL1

Display : No stored Option
Model Bin: 1-MAIN
Associated Worksheet: 1-WORKING_SHEET1

Units : SI

ABAQUS 4-8-4 : *STATIC, DIRECT

LOADCASE:1 TIMESTEP:1 TIME: 1.0

FRAME OF REF: GLOBAL

STRESS - XY MIN:-8828.14 MAX: 7418.03

Sealer/SWC Interface

7418.03

3000.00

2500.00

2000.00

1500.00

1000.00

500.00

0.00

-500.00

-1000.00

-1500.00 Y

-8828.14

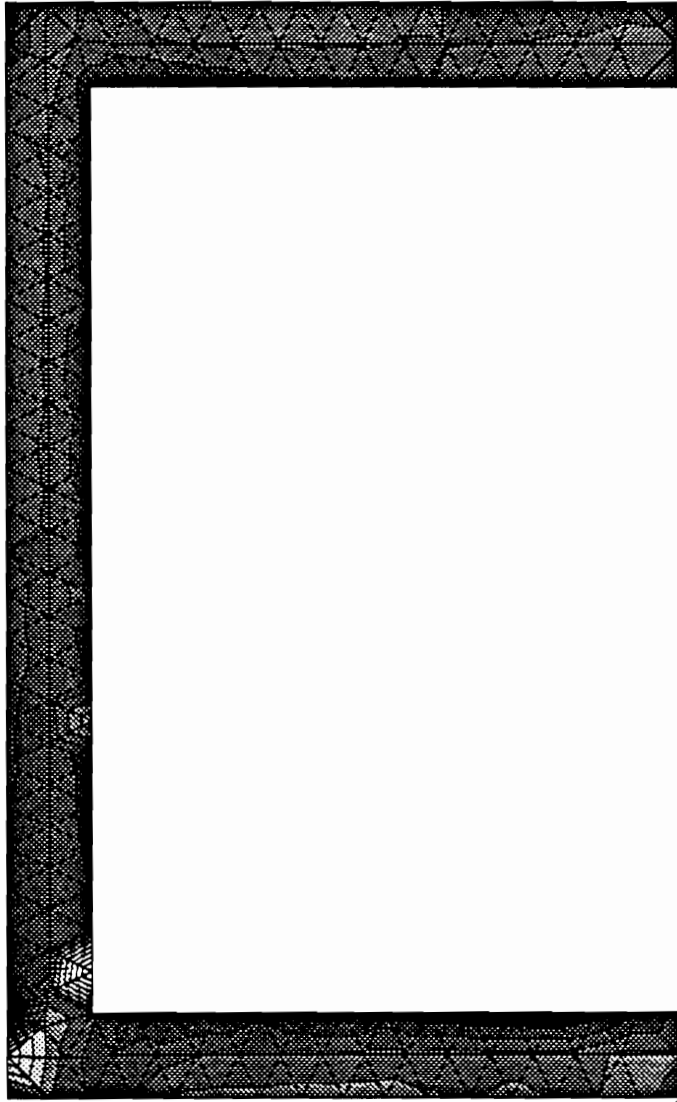
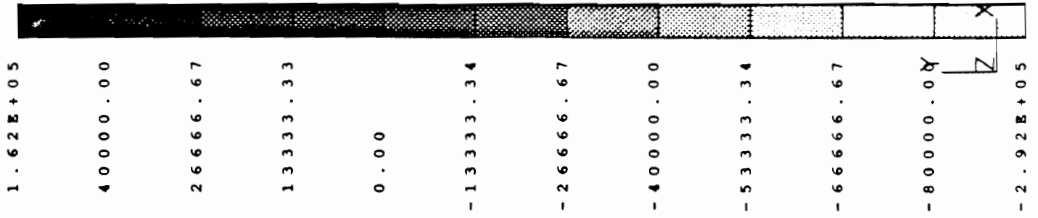
Database: Sealer E-Skel Torsion
View : No stored View
Task: Post Processing
Model: 1-FE MODEL1

Units : SI
Display : No stored Option
Model Bln: 1-MAIN
Associated Worksheet: 1-WORKING SET1

ABAQUS 4-8-4 : *STATIC, DIRECT

LOADCASE:1 TIMESTEP:1 TIME: 1.0
FRAME OF REF:GLOBAL
STRESS - Z MIN:-2.92E+05 MAX: 1.62E+05

Sealer/SWC Interface



VITA

Haruhiko (Harry) Kon was born on January 25, 1965 in Bethesda, Maryland to Hideo and Eiko Kon. After graduating from Walter Johnson High School in Bethesda in 1983, he attended Virginia Polytechnic Institute & State University where in 1988 he received his B.S. degree in Engineering Science & Mechanics. Deciding to continue his education, he remained at VPI & SU, studied adhesion science and received his M.S. degree in Engineering Mechanics in 1991.

Harry is currently pursuing a career in the automotive industry with Ford Motor Company's Body Engineering Division in the Materials & Corrosion Protection Engineering Department in Dearborn, Michigan.